VYSOKÉ UČENÍ TECHNICKÉ V BRNĚ
BRNO UNIVERSITY OF TECHNOLOGY

FAKULTA STROJNÍHO INŽENÝRSTVÍ
FACULTY OF MECHANICAL ENGINEERING

ÚSTAV FYZIKÁLNÍHO INŽENÝRSTVÍ
INSTITUTE OF PHYSICAL ENGINEERING

TOMOGRAFICKÉ MĚŘENÍ PRŮMYSLOVÝCH DÍLŮ PŘI TEPLOTÁCH POD BODEM MRAZU

TOMOGRAPHIC MEASUREMENT OF INDUSTRIAL PARTS AT TEMPERATURE BELOW FREEZING POINT

DIPLOMOVÁ PRÁCE
MASTER'S THESIS

AUTOR PRÁCE — **Bc. Rudolf Šárközi**
AUTHOR

VEDOUCÍ PRÁCE — **Ing. Tomáš Zikmund, Ph.D.**
SUPERVISOR

BRNO 2017

VYSOKÉ UČENÍ TECHNICKÉ V BRNĚ
FAKULTA STROJNÍHO INŽENÝRSTVÍ

Zadání diplomové práce

Ústav:	Ústav fyzikálního inženýrství
Student:	**Bc. Rudolf Šárközi**
Studijní program:	Aplikované vědy v inženýrství
Studijní obor:	Fyzikální inženýrství a nanotechnologie
Vedoucí práce:	**Ing. Tomáš Zikmund, Ph.D.**
Akademický rok:	2016/17

Ředitel ústavu Vám v souladu se zákonem č.111/1998 o vysokých školách a se Studijním a zkušebním řádem VUT v Brně určuje následující téma diplomové práce:

Tomografické měření průmyslových dílů při teplotách pod bodem mrazu

Stručná charakteristika problematiky úkolu:

Absorpční rentgenová počítačová tomografie (CT) je nyní úspěšně využívaná technika pro nedestruktivní charakterizaci vnitřní struktury materiálu jak v průmyslu, tak i ve vědě. Většina měření pomocí CT probíhá při pokojové teplotě v klimatizované komoře tomografu. V průmyslu se však vyskytují případy, kdy je třeba díly měřit při specifických teplotách. Při zvýšené nebo naopak extrémně snížené teplotě dochází k deformacím dílů, které je pomocí CT možné nedestruktivně odhalit. Takové měření je poměrně náročné, protože musí být dosaženo požadované teploty měření a tato konstantní teplota musí být udržena po dobu celého měření. Zároveň je nutné využít takové prostředky a materiály, které neovlivní nebo dokonce neznemožní CT měření.

Cíle diplomové práce:

- Seznámit se s rentgenovou počítačovou tomografií.
- Seznámit se současným řešením chlazení dílů pro rentgenovou počítačovou tomografii.
- Analýza současného stavu řešení (použité metody, materiály, atd.).
- Návrh úprav v použitých materiálech a metodách.
- Tomografické měření na průmyslové stanici GE L240.
- srovnání dat s měřením při pokojové teplotě

Seznam doporučené literatury:

KAK, A. C., SSLANEY, M. (1999): Principles of Computerized Tomographic Imaging. IEEE Press, Inc., New York.

HSIEH J.: Computed tomography: principles, design, artefacts, and recent advances, second edition, 2009.

Termín odevzdání diplomové práce je stanoven časovým plánem akademického roku 2016/17

V Brně dne:

L.S.

Prof. RNDr. Tomáš Šikola, CSc. ředitel ústavu	doc. Ing. Jaroslav Katolický, Ph.D. děkan fakulty

Abstract

X-ray computed tomography presents and ultimate for non-destructive investigation of objects. Under normal circumstances is the object placed on stage and the temperature of the object is defined by ambient air. However there are also cases when observation at freezing or high temperatures is needed to reveal thermal stability of observed object. Naturally the size of used tomography equipment and the object just like form of cooling or heating are subjected to final design. This work provides a summary of used methods for temperature controlled tomography. Furthermore handles about design of cooling chamber capable to reach $-40\,^{\circ}\mathrm{C}$ by preserving relative high X-ray transparency. As an addition that showed up as a response to additional requirements is here presented a heating chamber, in which the object can be maintained at $80\,^{\circ}\mathrm{C}$. All test and scans were carried out on GE phoenix v|tome|x L240 industrial computed tomography scanner.

Keywords

X-ray Computed tomography, chamber, freezing point , $-40\,^{\circ}\mathrm{C}$, $80\,^{\circ}\mathrm{C}$

Abstrakt

Röntgenová počítačová tomografia je ultimátnym nástrojom umožňujúcim nedeštruktívnu analýzu objektov. Za normálnych okolností je objekt umiestnený na podstavec a teplota objektu je daná teplotou okolitého vzduchu. Existujú však prípady kedy je žiaduce skenovanie za nízkych prípadne vysokých teplôt za účelom odhalenia tepelnej stability objektu. Samotné riešenie je do veľkej miery podradené rozmerom samotného zariadenia a vzorky ako aj zvolenému spôsobu ohrevu a chladenia. Táto práca podáva prehľad už použitých spôsobov pre tomografiu za kontrolovanej teploty. Okrem toho sa v tejto práci nachádza aj návrh komory umožňujúcej dosiahnuť $-40\,^{\circ}\mathrm{C}$ pri zachovaní vysokej transparentnosti pre Röntgenovo žiarenie. Ako dodatok vyplývajúci s dodatočných okolností je v tejto práci aj návrh komory umožňujúcej ohriať vzorku na $80\,^{\circ}\mathrm{C}$. Všetky testy a merania prebiehali na prístroji GE phoenix v|tome|x L240

Kľúčové slová

Röntgenová počítačová tomografia,komora, bod mrazu, $-40\,^{\circ}\mathrm{C}$, $80\,^{\circ}\mathrm{C}$

Bibliografická citácia

ŠÁRKÖZI, Rudolf. *Tomografické měření průmyslových dílů při teplotách pod bodem mrazu*. Brno, 2017. 67s. Diplomová práca. Vysoké učení technické v Brně. Fakulta strojního inženýrství. Vedoucí práce Tomáš ZIKMUND.

Čestné prehlásenie

Čestne prehlasujem, že diplomovú prácu na tému *Tomografické měření průmyslových dílů při teplotách pod bodem mrazu* a všetky prílohy som vypracoval samostatne a uviedol som všetky použité zdroje a literatúru.

V Brne dňa 20.5.2017

Rudolf Šárközi

Poďakovanie

Na tomto miesto by som sa rád poďakoval tímu pracujúcemu okolo CT prístroja a obzvlášť Michalovi Petrilakovi a Martinovi Karešovi za ich vrúcny prístup a pomoc ako pri skenovaní tak pri následnom spracovaní obrazu. Ďalej moja vďaka patrí mojej rodine ktorá ma vždy podporovala a mojej priateľke Carmen ktorá mi je vždy oporou.

Contents

Introduction

Computed tomography (CT) represents a very powerful tool of non-invasive analysis. Although it is famous mostly for its medical application, the industrial usage also gained its irreplaceable reputation as an analysis technique. The Requirements on Computed tomography are still increasing, forcing the developers for better machines and more sophisticated software. Moreover, an analysis of samples under various environmental conditions is required. Plenty of parts from various industry fields have to withstand wide range of temperatures. Most of materials slightly retract by temperatures far beneath 0 °C and expand by relatively high temperatures. This process can lead to deformations that can slightly change the shape of the part, which makes it unusable for previous purpose. Tomography can reveal the most temperature sensitive part of sample giving feedback to a manufacturer how to change the original design. However, most of CT machines cannot be placed into chamber with −40 °C, whether it is technically too difficult or it is too expensive. Therefore we came up with a polystyrene chamber where we can reach −40 °C for a time necessary for a high resolution scan with using a special coolant. Besides we constructed sample holder to keep the sample fixed inside the chamber. The first test revealed the need for a new chamber, whose shape was optimized using FEM analysis. Meanwhile we came up with idea of a hot chamber, in which we would maintain 80 °C. That of course meant way different requirements for materials and heat production. In few weeks also the hot chamber was finished. It was made from double wall fibreglass corpus filled with flame resistant polyurethane foam and equipped with electrical heat source that was controlled by thermostat. It is also necessary to say that the main requirement for both chambers was a very high X-ray transparency. As a reference sample a car door handle was used and the scan under various temperatures was taken. Results are discussed in conclusion.

1 Historical overview

1.1 Roentgen Radiation

The history of computed tomography began with discovery of Roentgen radiation. It was first observed and described by the German experimental physicist Wilhelm Conrad Röntgen in 1895, while he was studying the so called cathode radiation. This radiation occurred in vacuum tube [1] between two charged plates. At that time scientific world was not sure what cathode rays actually were. Now we know, thanks to J.J.Thomson, that cathode rays are electrons, and as they pass through low pressured air they ionize present atoms causing illuminating radiation. But Wilhelm observed another type of radiation also bounded with electron movement and since they decelerate on vacuum anode interface, they emit X-rays. Röntgen referred to the radiation as "X", to indicate that it was an unknown type of radiation. The name is used often also nowadays, although many of his colleagues suggested calling them Röntgen rays. Six year after publishing his work in year 1901 Wilhelm received the Nobel prize for Physics. It was also the first Nobel Prize for Physics in history.

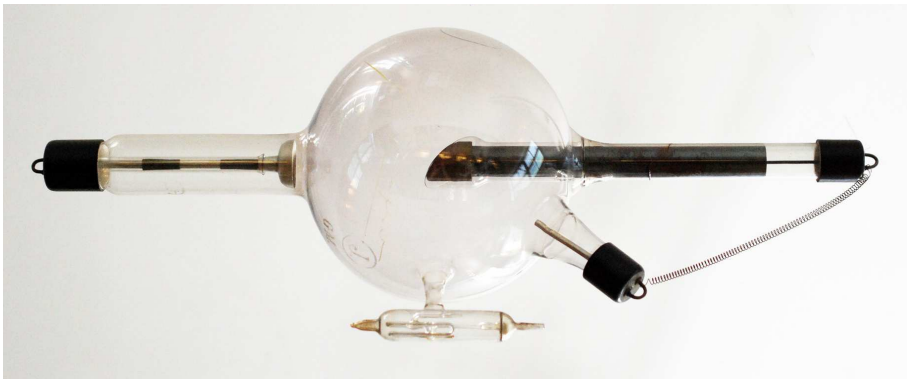

Figure 1: An early Crookes X-ray tube from a museum dedicated to Wilhelm Conrad Röntgen in Würzburg (GNU free documentation license).

[1] Vacuum in that time was not very good, actually it was a tube with slightly lower pressure than atmospheric. Wilhelm used Crookes tubes invented by the British physicist William Crookes by improving mechanism of that time used mercury pump. With this equipment he was able (depending on circumstances) to reach pressure up to $10^{-5} - 10^{-6}$ atmospheres (10-0.1 Pa).

This type of radiation has also a very interesting capability which changed the medicine world almost overnight. Röntgen had covered his tube with black cardboard to block the distracting glow caused by electrons striking the tube glass walls. To his surprise, he noticed out of the corner of his eye that a fluorescent screen placed more than a meter away was also glowing. X rays were able to penetrate to most solids depending on the object's density. He published his observations and mailed his colleagues a photograph of the bones of his wife's hand, showing her wedding ring on her fourth finger.

Figure 2: Image of Röntgen's wife's hand, on December 22, 1895, shortly after discovery of X-rays. [1]

1.2 Computed tomography

It did not last long and Glasgow hospital opened a radiology department. People were able to observe kidney stones or a penny stacked in throat without harming a patient. It meant a huge breakthrough but the image from X-ray examination allowed only two dimensional analysis and people started to think of a new method to get more information about internal structure. A Polish doctor Karol Mayer came up with one of significant improvements in year 1916 [2]. He obtained X-ray images using a moving X-ray tube and a stationary film cassette. This method resemble a technique used in modern tomography and his acknowledgements are considered to be the prelude to Tomography. Unfortunately, to obtain a correct three dimensional image a big amount of calculations and image transformations has to be done.

This fact slowed down the development of tomography till early 60s when the first computers showed up. Modern Computed Tomography is a result of work of two men. The first of them is the South African Allan MacLeod Cormack and the other one is the English Godfrey Newbold Hounsfield. Cormack studied absorption of X-rays by biological active materials using the aparatus built by himself. His approach was more theoretical and in 1963 he published his results in paper, called Representation of a Function by its Line Integrals [3], which represents a basis for an image analysis in tomography. This work lay a few years without a big interest till Hounsfield came up with his first tomography machine. Hounsfield during w.w.II worked on radar development for air defense. Skills obtained during this work undoubtedly helped him later by developing the first tomography equipment. At first he used gamma radiation from americium (Am) but the intensity was too weak and the exposure took a very long time. The whole scan of human brain in formalin lasted almost nine days and the image had a resolution 80×80 pixels.

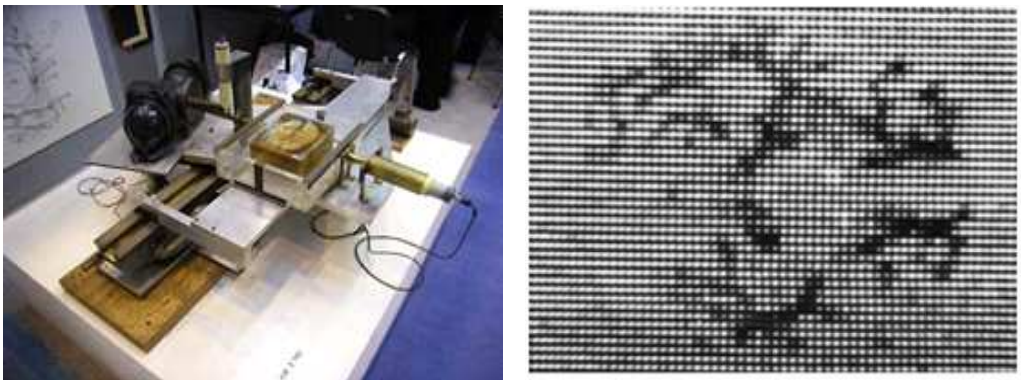

(a) (b)

Figure 3: An original apparatus used by Hounsfield (a) and scan of human brain by this aparatus (b),source: [2]

When Hounsfield changed gamma radiation for X-rays he was able to shorten the exposure time significantly.The actual process of image reconstruction was reduced to 20 minutes. In September 1971 with the help of two neurologist James Ambros and Louis Kreel was placed in Morley Atkinson Hospital in Wimbledon the first commercial CT scanner named EMI Mark I [2].

Despite of the fact that tomography principle was invented much earlier (in 1826) by Norwegian mathematician Niels Henrik Abel [4] and the theory of line integrals for function representation by Cormack

was developed much further by the Austrian Mathematician Johan Radon already in 1917 [5], it is used till nowadays. It is the Solution presented in cooperation of Cormack and Hounsfield, that fully deserves the name Computed tomography and for their contribution they received a Nobel Prize for Physiology and Medicine in 1979 [6].

Figure 4: Men of Tomography with their scanners.On the left Allan MacLeod Cormack and on the right Godfrey Newbold Hounsfield

2 X-ray production

Röntgen radiation could be exploited and studied fast since its discovery thank to the relative simplicity of the equipment needed for its generation. However higher demands on intensity and focusing ability led to development of more sophisticated and in most ways more complex sources and detectors. This chapter deals with Physics connected with X-rays generation, X-ray-matter interaction and some general properties of this type of radiation. This chapter first of all focuses on features important for computed tomography and in any manner contemplates to become a complete guide for X-rays production and detection. X-ray radiation is a part of electromagnetic spectrum between ultraviolet and gamma radiation as shown in the following scheme:

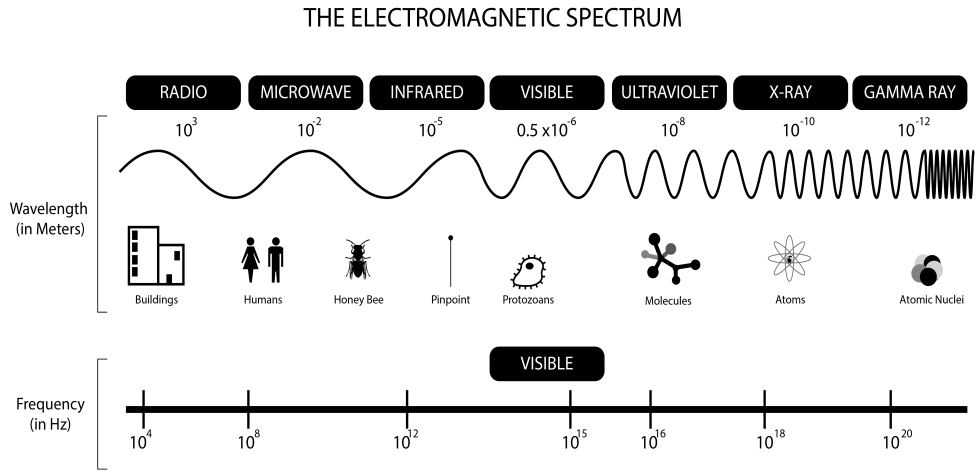

Figure 5: Electromagnetic Spectrum,source:wikimedia

The Wavelength of this radiation is comparable with interatomic distances 1-10 Å [2] for so called soft X-rays and 0.1-1 Å for so called hard X-rays. That's also the reason why this radiation is used in crystallography for crystal structure determination. Its comparability with interatomic distances give rise to strong diffraction effects that are used for precise crystal structure measurements. However for CT purpose is another virtue of this radiation crucial, and concretely its ability to penetrate through materials with relative low density, like organic tissues wood or plastics which are mostly opaque for visible light.

[2] Angström = 10^{-10} m

2.1 X-ray sources

The most common X-ray source is in principle similar to the source used by Wilhelm Röntgen. Nowadays this equipment is much more sophisticated but the principle remains.An evacuated tube with two electrodes held on relatively high potential difference. The intensity of the produced X-rays is proportional to the atomic number of the target material and to the number of electrons bombarding the target. As a cathode usually a tungsten filament is used, heated on high temperatures, approx. 2700 °C.

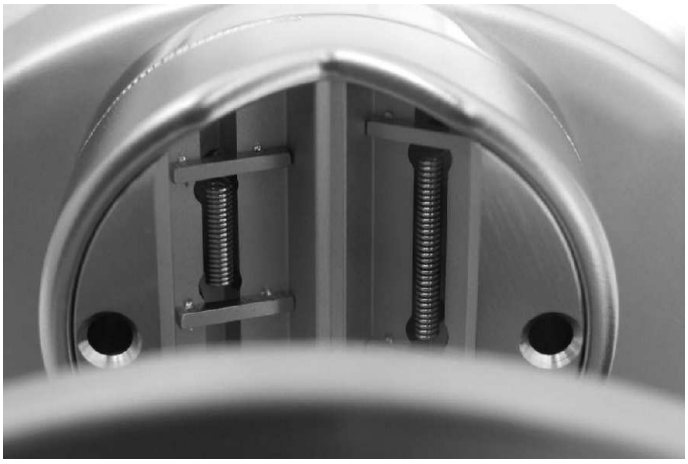

Figure 6: Cathode filaments (kept at approx. 2700 °C).The larger filament generates bigger spot on anode to obtain more intensity. Smaller filament generates smaller spot with less intensity but more monochromatic. Tabs at the end in length direction shorten the focal spot and homogenize the electron intensity distribution. There is so called Wehnelt cylinder around both filaments. It's held on negative potential and works as a focusing lens for electrons. source: [7]

High temperature raises the energy of electrons and enables them to overcome energy barrier called also a work function to leave the material. This process is called thermal emission and the current density generated by thermionic source is described by Richardson law [8].Consequently the electrons from cathode are accelerated towards anode but near it's surface a strong coulombic repulsion takes place, forcing the electrons to decelerate giving rise to radiation according to laws of electromagnetism. This deceleration process usually emerges several photons from one electron. There is also a certain probability that the whole energy of electron is transformed into photon which allows us to determine minimal radiation wavelength λ_{min}.

$$eU = hf_{max} = E_{max} \tag{1}$$

$$\lambda_{min} = \frac{hc}{E_{max}} = \frac{1.24\,\mathrm{nm}}{U[\mathrm{kV}]} \tag{2}$$

Where e is elemental charge, U accelerating voltage, h plank constant, f_{max} maximal radiation frequency and c is speed of light. While by voltage we can determine the out highest energy of out-coming spectrum, the intensity of radiation depends on current density of electron beam.

However, electrons in beam have a certain energy spread and the deceleration process involves multiple interactions (as seen in figure 7). Due to this fact, an emerging radiation shows a continuous energy spectrum called also Bremsstrahlung[3].

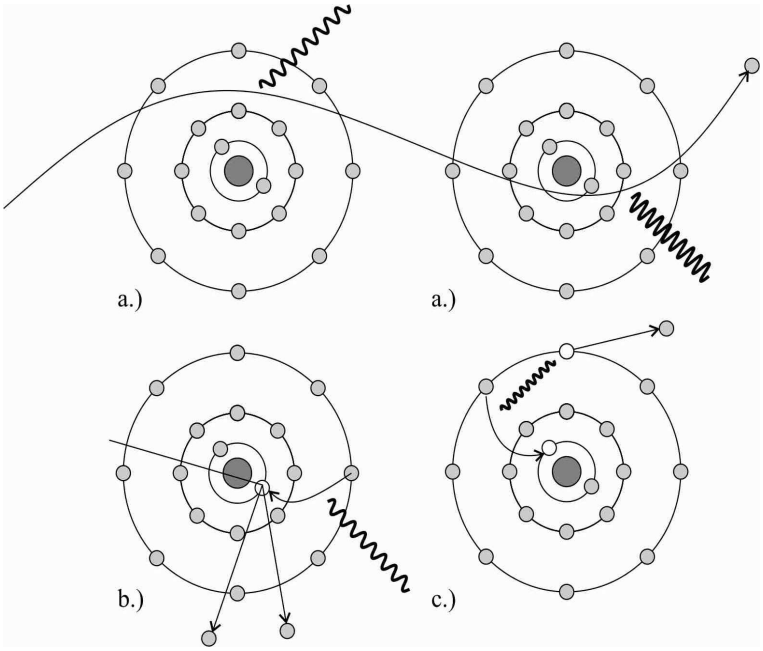

Figure 7: Various interactions of an electron with an atom (there are much more of them like fluorescence exitation and so on), a.) Represents a Bremsstrahlung caused by deflection, the nearer the electron passes the nucleus the stronger deflection occurs, which means more energetic photon is being radiated. Case b.) represents a characteristic radiation and c.) auger electron emission, [9].

[3]From German Bremsstrahlung - Brake Radiation

2.2 Characteristic radiation

During electron-matter interaction a characteristic X-ray radiation also occurs, which is superimposed on background formed by Bremsstrahlung. As the name suggests, characteristic radiation is unique for every element which the electrons impact. An atomic electron can be "kicked out" from inner atomic shells (figure 7b.)) by interaction between atom and high accelerated electron [4]. This destabilizes the atom leading to electron reorganization. Mostly electron from higher shells fall to lower shells and a quantum of energy is radiated out. Energy of this radiation corresponds to an energy difference between shells.

$$E_k(e^-_{in}) = E_k(e^-_{atom}) + hf \tag{3}$$

An element with a relatively high atomic number is necessary to obtain a high energy radiation, because the energy difference between the highest and the lowest shells of light elements isn't big enough to give rise to radiation in Röntgen's spectrum and the probability of radiation rises with the rising atomic number. Wavelength of outcoming radiation is given by difference between the higher and the lower shell E_h and E_l:

$$\lambda = \frac{hc}{E_h - E_l} \tag{4}$$

2.2.1 Beam Filtering

The presence of more wavelengths in produced spectrum causes a set of unwanted effects. Tomography requires radiation as monochromatic as possible, otherwise we have to deal with unwanted effects, like beam hardening (see below). To fulfil this requirement, a synchrotron radiation can be used for special purposes [5]. There is also a possibility to filter tube radiation using light elements due to their ability to absorb relatively weak and low energetic bremsstrahlung. To filter one of the characteristic peaks in spectrum an element with appropriate absorption has to be used(figure 8). For example, copper strongly radiates at 1.54 and 1.39 Å (K_α and K_β) but Nickel absorbs strongly till 1.49 Å so it can absorb almost 100 of K_β intensity peak but lets almost 50 of K_α peak going through. Thus, a copper X-ray source with a nickel filter can produce a nearly monochromatic X-ray beam with photons of mostly 1.54 Å

[4] It can also be another particle, for example alpha particle, photon and others

[5] Synchrotron radiation occurs when charged particle is moving in circle trajectory. Particle radiates a well-defined radiation in direction tangent to trajectory [10]

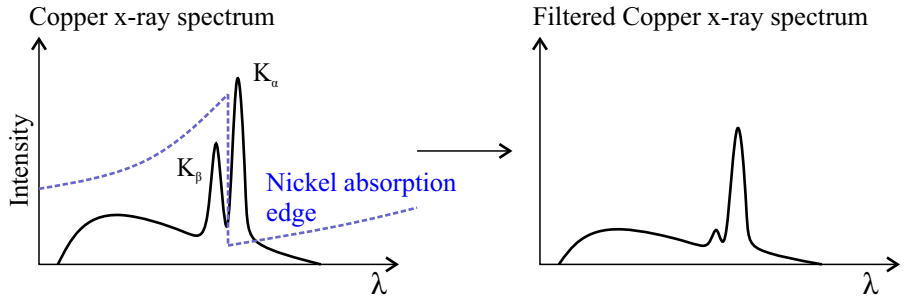

Figure 8: On the left, there is an unfiltered simplified spectrum of copper anode. On the right, it is a filtered spectrum using nickel plate filter.

Beam hardening
The X-ray absorption by matter tends to decrease for incident photons of greater energy causing an effect that is called beam hardening [11]. It occurs because the amount of attenuation inside the material depends on the wavelength of radiation, and mostly in strong absorbing media the less energetic radiation (longer wavelength) is being strongly attenuated than the more energetic. This fact causes that on detector surface impact only rays of shorter wavelength (hard radiation). As a result the edges of objects are much brighter than the center, which can lead to misinterpretation during reconstruction. There are more ways how to restrict this effect. One of them is to cover the X-ray source with a thin metal plate and makes the beam "harder" already before sample. There also exist reconstruction algorithms that are able to minimize the influence of beam hardening but the universal method for every sample doesn't exist and the ways of dealing with beam hardening are still discussed in tomography papers.

2.2.2 Thermal dissipation

As seen on figure 8 characteristic peaks form only a few percent of the whole emerging radiation. Most of the spectrum is built of Bremsstrahlung. Unfortunately the conversion rate of kinetic energy of electrons to X-ray radiation is relatively small and can be estimated using following formula [6] :

$$\eta = KZU[kV] \tag{5}$$

[6]This equation also means that the elements with higher Z have a higher conversion efficiency

Where Z is an atomic number, U is the accelerating voltage in kilovolts and K represents constant of value $K = 9.2 \times 10^{-7} kV^{-1}$ theoretically found by Kramer [2]. Effectiveness of X-ray conversion on tungsten anode ($Z = 74$) with potential difference 140 V is slightly above 1%. Rest is converted to heat.

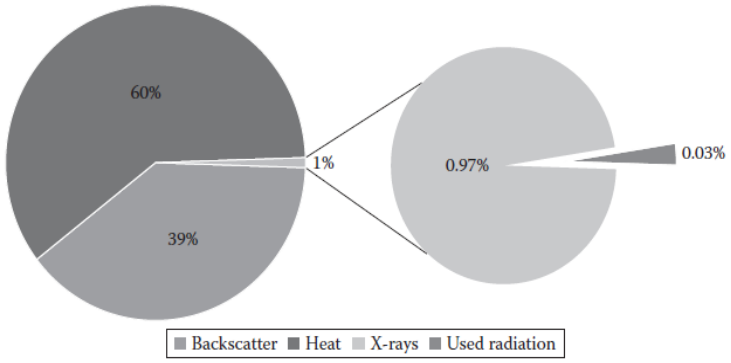

Figure 9: Share of power for the most relevant processes during electron impact in tungsten, [12]

In tomography accelerating voltages from 80 up to 300 kV are used. For example device in our laboratory operates with 320 W of energy. It doesn't seem too much but this power is focused in a very small focal point. This amount of thermal dissipation would normally lead to melting of every kind of material. Fortunately, this problem can be solved by a rotating cathode made from a material with high melting point (commonly graphite). This cathode is covered with desired material and rotates with frequency about 3000 rpm depending on type. Therefore, the electron beam forms a focal circle instead of a point leading to better heat dissipation. The scheme of rotating cathode tube is displayed on the following picture.

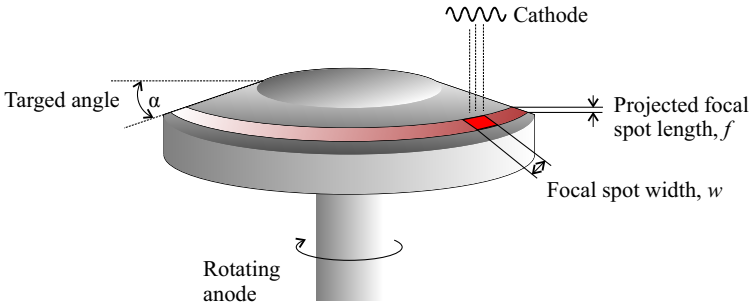

Figure 10: Scheme of rotating anode

2.3 Micro-focus Tube

For purposes of computed tomography should be the source of radiation point like. Broader source leads to unwanted fragments in image like for example so called *penumbra* [13].The image affected by this error has blurred edges as if the radiation came from more sources. X-ray tubes are subjected to European Standard Norms (EN) that declares the quality of various types of tubes. Micro and mini focus tube parameters are involved in norm EN 12543-5. Our equipment (GE phoenix v—tome—x L240) is equipped with 240 kV micro focus tube that fall within this norm.

3 X-ray Detection

Photographic paper as a basic type of X-ray detector was already used by Wilhelm Röntgen himself during his discovery. Photosensitive paper is used also nowadays in hospitals for a simple selective two dimensional projection of X-ray. This type of detection provides information about intensity distribution of X-ray passing through specimen (or patient) but requires a relatively long exposition time to obtain good resolution. However computed tomography requires sources with digital output because that is the requirement for the computer processing of a detected signal. To fulfil these requirements X-rays have to be converted to electrons.

3.1 Scintillator detector

Scintillators represent a major class of detectors used in nuclear medicine and sciences. Scintillator crystals are able to convert the incoming X-ray radiation to ultraviolet or even visible part of spectrum and it is consequently detected by photomultiplier or photodiode. They are based on photoelectric effect. The X-ray photons knock out electron in scintillator material which leads to fluorescence decay. Common materials for crystals are cesium iodine (CsI) cadmium tungstate (CdWO4) or bismuth germanate (BGO) [14]. Important material factor here is the quantum efficiency of conversion (QE) that describes how effectively the material converts certain wavelength. To obtain the best output is desired to compensate weak QE of electron detector in certain region with high QE of used light detector. Modern CT devices also require a very short conversion time (very fast fluorescence flash). To fulfil these requirements ceramic materials made of rare element oxides like gadolinium oxysulphide (Gd2O2S) [7] are used.

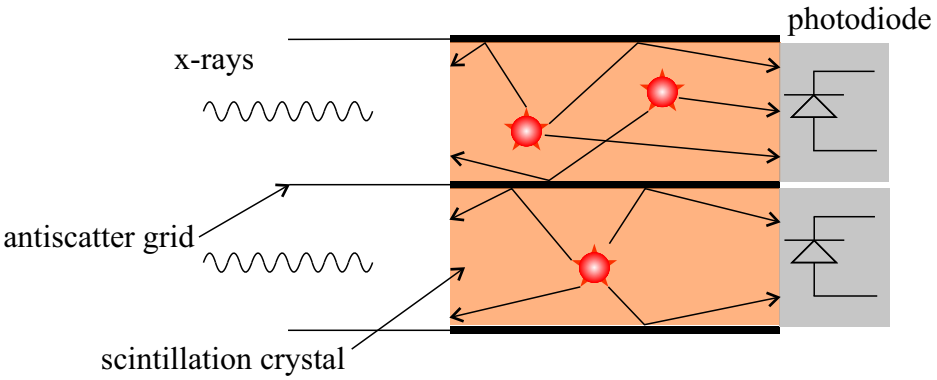

Figure 11: Scheme of Scintillator detector

The Thickness of scintillation crystal is about 1-2 mm and is shaped to illuminate mostly rear wall of the crystal oriented to detector. Antiscatter grid suppresses rays scattered through small angles. These rays are undesired because they reduce the image contrast. However, it decreases geometrical effectivity of detector that leads to lower spatial resolution.

3.2 Flat panel detector

Scintillator detectors above can be extended to a matrix that forms a detector panel.The advantage of this setup is the maximum of X-ray sensitive area. Modern CT devices are mostly equipped with this type of detectors due to their high sensitivity and large sensitive area that significantly abbreviates time required to acquisition compared to row detectors.

Figure 12: Flat panel detector of our GE phoenix v—tome—x L 240 tomography machine

4 X-ray matter interaction

X-rays are known to have a relatively high capability of penetration (depending on material). However, the number of photons decreases exponentially as ray passes through a material. It is caused by scattering and absorption processes. Therefore in this chapter the Physics of photon-mater interaction that stand for radiation attenuation is briefly discussed. Loss in intensity along a beam axis characterizes the observed specimen and represents essential information for tomography.

4.1 Lambert-Beer's Law

In order to understand attenuation in matter, let's assume that we have a monochromatic beam.The intensity of the beam can be defined as:

$$I = \frac{N_{photons} h f}{St} \tag{6}$$

Where $N_{photons}$ represents the number of photons, h is Planck's constant and f is the frequency of used radiation. In denominator area S is multiplied by time t. Let's consider an incoming radiation of intensity I_0. After passing through distance Δx, intensity decreases proportionally to this distance multiplied by a factor defining the material $\mu(x)$.

$$I(x + \Delta x) = I(x) - \mu(x) I(x) \Delta x \tag{7}$$

Reordered to obtain $\mu(x)$

$$-\mu(x) I(x) = \frac{I(x + \Delta x) - I(x)}{\Delta x} \tag{8}$$

Taking $\Delta x \to 0$ leads to differential equation

$$\lim_{\Delta x \to 0} \frac{I(x + \Delta x) - I(x)}{\Delta x} = \frac{dI}{dx} = -\mu(x) I(x) \tag{9}$$

That has the following general solution

$$I(x) = e^{-\mu(x)x + C} \tag{10}$$

The integration constant C can be determined from the condition that before material we have considered intensity I_0, so when we join the coordinate system with edges of the material $I(0) = I_0$ we obtain:

$$I(x) = I_0 e^{-\mu(x)x} \tag{11}$$

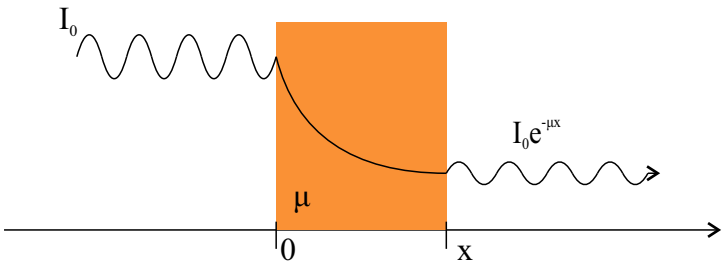

Figure 13: Illustration of Lambert-Beer's law, exponential decrease of intensity as beam passes through material is defined by $\mu(x)$

This equation is known as Lambert-Beer's law and determines the intensity of radiation loss after passing through matter [15]. The value of attenuation coefficient $\mu(x)$ involves losses due to scattering but also due to absorption. However, $\mu(x)$ is generally a function of spatial variables x,y,z that depends mostly on the releavant density distribution of the material. Main goal of tomography is to obtain this function from individual projections in order to get attenuation distribution of object which is then correlated to structural and material composition. That is content of following chapter about image reconstruction.

5 Image Reconstruction

Today, CT systems use fan-beam geometry. However, it is more instructive to introduce CT reconstruction using simple parallel beam geometry, in which, for every direction of projection, the X-ray beam is collimated to a straight ray and moved linearly in the direction parallel to a linear X-ray detector array. This concept was typical for first generation of CT systems [2]. Sequentially, the X-ray sampling unit is rotated by an angle θ, and, subsequently, moved linearly. This process is repeated until any point of the object to be reconstructed is illuminated by at least 180 degrees. Figure 14 shows this sampling process schematically.

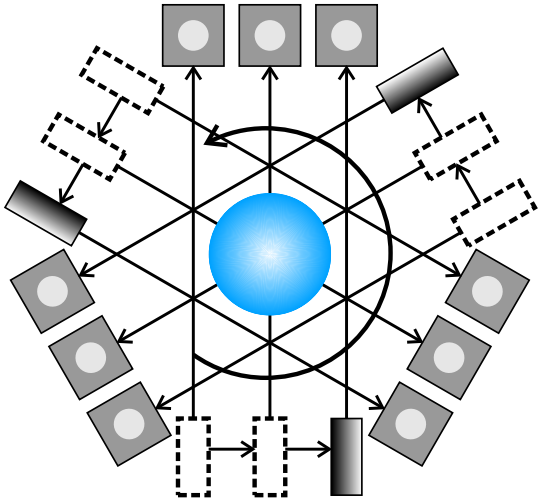

Figure 14: Schematic drawing of parallel beam geometry in first-generation CT systems

As X-rays travel a line p from the X-ray source through the object to a detector, they are attenuated by the material on this line. According to Lambert-Beer's law, the X-rays at a certain point are attenuated proportionally to attenuation coefficient μ. If the X-rays are monochromatic, then the linear attenuation coefficient is proportional to the density of the object. Amount of attenuation $q(p)$ is a sum of single attenuations along the ray path of length P. When we differentiate the path to infinitesimal parts dp we can express intensity decrease for single ray as a projection integral[7] under a certain angle θ:

$$q_\theta(p) = \int_0^P \mu dp \tag{12}$$

[7]If the attenuation coefficient changes steps like the integral is replaced by sum.

Then the decrease in intensity in every detector pixel can be expressed as:

$$I_\theta(p) = I_0 e^{-\int_0^P \mu dp} = I_0 e^{-q_\theta(P)} \tag{13}$$

Where I_0 is the intensity of source and $I(p)$ represents the intensity of the radiation that travelled through the path p inside the specimen.
Real samples are mostly heterogeneous and we have to replace attenuation coefficient μ (which is in that case a constant defined for material) for attenuation function $\mu(x, y)$. Our goal is to obtain $\mu(x, y)$, which is quantity of fundamental significance for image reconstruction. Mathematically expressed[8] we transform a continuous function of two variables defined on compact space into a form expressed by line integral along each straight line that is represented by X-ray. In our case the transformed function is attenuation function $\mu(x, y)$ and the compact space is defined by observed object. This process is described by so called Radon transform [16] defined for given ray path p of length P by following formula:

$$R : \mu(x, y) = \int_0^P \mu(x, y) dp \tag{14}$$

From equation 13 follows:

$$R : \mu(x, y) = \int_0^P \mu(x, y) dp = \ln \frac{I_\theta(p)}{I_0} \tag{15}$$

This integral transform is exactly the classical Radon transform of function $\mu(x, y)$ on the line p and since I_0 and $I(p)$ are measured, the line integral is known and the $\mu(x, y)$ can be computed. Complete tomographic data are X-ray data over all lines. In practice, this means that data are collected on a fairly evenly distributed set of lines throughout the object as can be seen in figure 15. However, according to figure 15 the path of ray is given by angle and distance from rotation center. Therefore we need to find a formula for converting from the fixed coordinate system (x, y) into the moving system (r, s), which is rotated by an angle θ with respect to the (x, y) system. Relationships in table 1 allow us to convert the coordinates of any point in the fixed coordinate system into coordinates in the moving system and vice versa. When we have these transformations we can express equation 13 in rotating coordinate system.

[8]Purpose of this expression isn't in any case to give proper mathematical definition, but just briefly explain meaning of this transformation. Rigorous description of Radon transform can be found for example in [16]

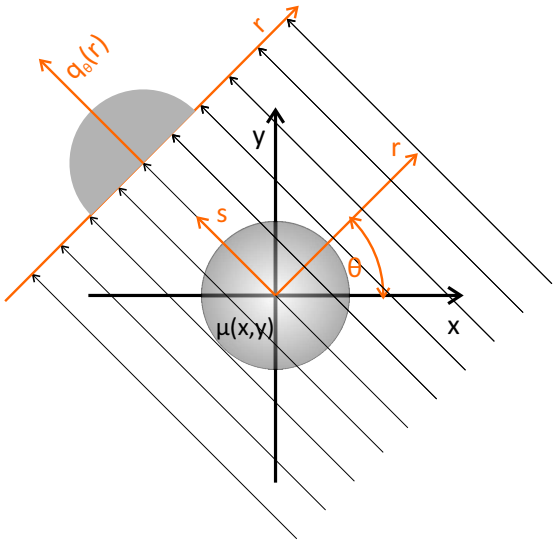

Figure 15: Scheme of simplified scanning geometry. Projections carried out under various angles θ create an intensity distribution on detector that can be described as a function of distance from rotation axis r. The rotation axis of scanner is placed inside object ($r = 0$)

Table 1: Trigonometric relations between static system (x,y) and rotating system (r,s)

$(x, y) \to (r, s)$	$(r, s) \to (x, y)$
$x = r\cos\theta - s\sin\theta$	$r = x\cos\theta + y\sin\theta$
$y = r\sin\theta + s\cos\theta$	$s = -x\sin\theta + y\cos\theta$

However, we cannot forget that every value of the quantity $q_\theta(r)$ (Subscript denotes the angle of projection) is a sum of absorptions along the ray path (line integral). In fact, this reflects the physical process of X-ray attenuation by matter. Therefore we have to integrate just over points along this path p as shown in figure 15. This fact will be secured using Dirac delta function [17] that sets to zero contributions from all points besides points on ray path p. Properly it can be written as follows:

$$q_\theta(r) = \mu(x, y) * \delta(p) = \iint_\Omega \mu(x, y)\delta(x\cos\theta + y\sin\theta - r)dxdy \qquad (16)$$

Since p is the path of X-ray photons for a certain position (r, θ) of the X-ray tube, the meaning of above equation is that all attenuation values in the material along the line p are integrated. Area of integration ω is formed by object boundaries. As we can see in figure 16 for parallel beam geometry is the position of X-ray tube and therefore position of path p given by r.

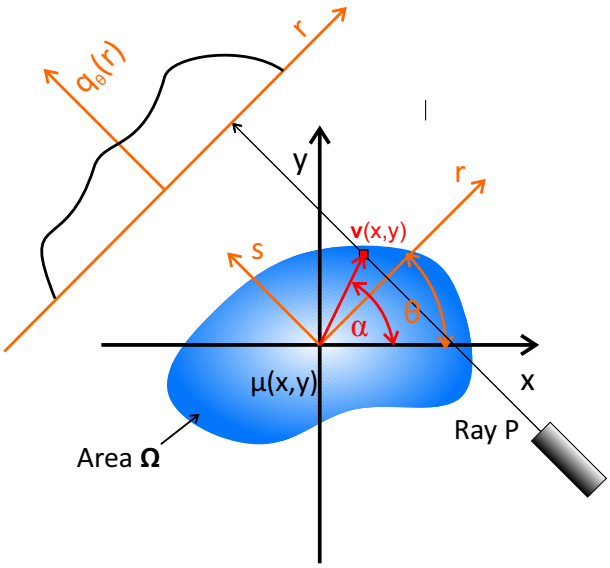

Figure 16: All points of the object lying on the line p are passed through by X-ray photons. The resulting exponential decay of the X-ray intensity is due to the attenuation values lying along this line.

Complete Radon transform of $\mu(x, y)$ represents an output dataset, that can be represented as matrix of $m \times n$ dimension, where m corresponds to vector $q(r)$ containing attenuation values for every X-ray tube step and n corresponds to number of projections under various angles. This matrix is usually represented in grayscale diagram. In this diagram the values of point that lie out of center forms a sinus shaped curve and therefore is it called a *sinogram*(figure 17).

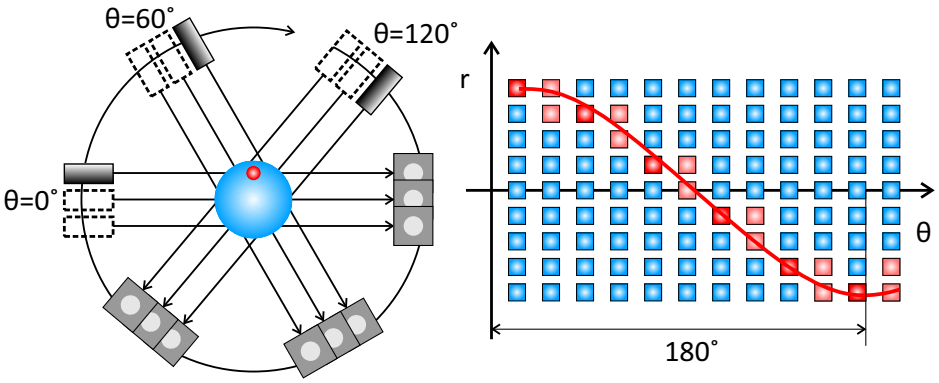

Figure 17: Representation of scan dataset as a matrix that contain values for every scan. Off axis points of object form the sinusoidal curve, therefore this representation is also called *sinogram*

5.1 Fourier Slice Theorem

To complete the image reconstruction we have to face the problem that was first formulated by Johann Radon self [18]. How to obtain spatial distribution of attenuation coefficient $\mu(x, y)$ having only single projections $q_\theta(r)$. To achieve this task, we use so called Fourier slice theorem [19]. Let's have a fixed projection angle θ_c. We obtain a projection corresponding to this angle $q_\theta(r)$. Although $q_\theta(r)$ is function depending on spatial variables, we would like to transform it into a "spatial frequency domain".

$$q_\theta(r) \rightarrow Q_\theta(\omega)$$

In can be done using Fourier transform

$$Q_\theta(\omega) = \int_{-\infty}^{\infty} q_\theta(r) e^{-2\pi i r\omega} dr \tag{17}$$

Using identity from equation 16 we obtain[9]

$$Q_\theta(\omega) = \int \left[\iint \mu(x, y)\delta(x\cos\theta + y\sin\theta - r)dxdy \right] e^{-2\pi i r\omega} dr \tag{18}$$

It can be reorganized to flowing form

$$Q_\theta(\omega) = \iint \mu(x, y) \left[\int \delta(x\cos\theta + y\sin\theta - r) e^{-2\pi i r\omega} dr \right] dxdy \tag{19}$$

[9]For simplicity we neglect integral boundaries

Dirac delta function defines exactly the set of x and y for which the integral isn't equal to zero, in other words, its non-zero only for x and y lying on ray path defined by $r = x\cos\theta + y\sin\theta$.

$$Q_\theta(\omega) = \iint \mu(x,y)e^{-2\pi i\omega(x\cos\theta + y\sin\theta)}dxdy \tag{20}$$

At this point is convenient to choose following substitution:

$$u = \omega\cos\theta$$
$$v = \omega\sin\theta$$

Using this substitution we obtain:

$$F(u,v) = \iint \mu(x,y)e^{-2\pi i(ux+vy)}dxdy \tag{21}$$

What we get is a 2D Fourier transform of attenuation function $\mu(x,y)$ evaluated along a line p .It is a very important fact because it means that Fourier transform of a single projection $q_{\theta_c}(r)$ under fixed angle θ_c is identical to the line in 2D Fourier transform of entire image (attenuation function $\mu(x,y)$) defined by this angle (figure 18).

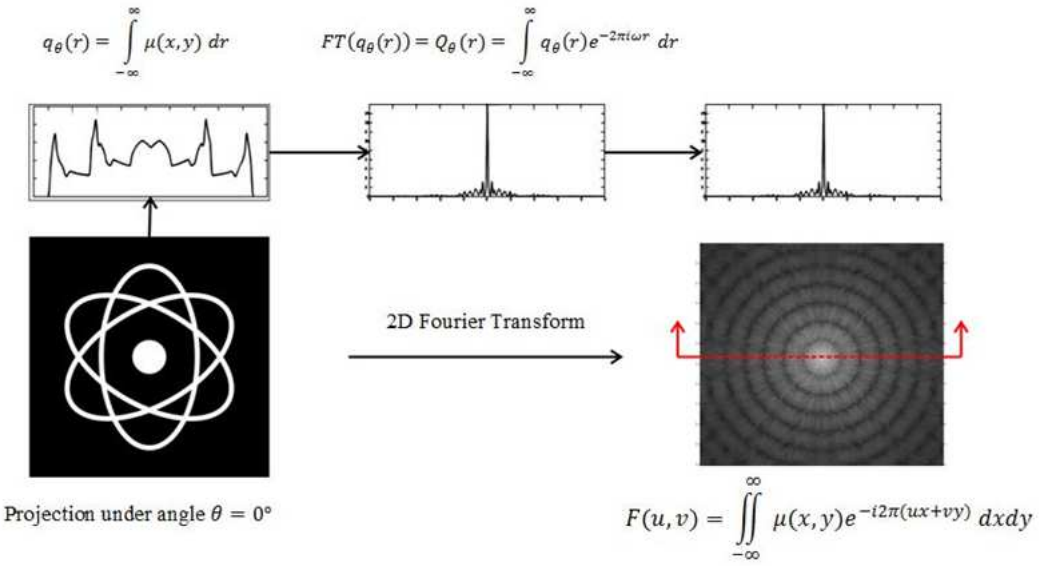

Figure 18: Demonstration of Fourier Slice Theorem calculated using MATLAB

This is a very helpful fact, because it tells us how to obtain the desired attenuation function $\mu(x, y)$ that correlates with structure of observed object. We can transform all obtained projections and we get the 2D Fourier transform of the original function. Then just apply inverse Fourier transform and obtain original image (function of attenuation). But unfortunately the sampling pattern produced in the Fourier space is non-Cartesian. The Fourier slice theorem states that the Fourier transform of a projection is a line through the origin in 2D Fourier space, which means that the Centre of image is oversampled while towards the edges the sample rate decreases as shown in following figure:

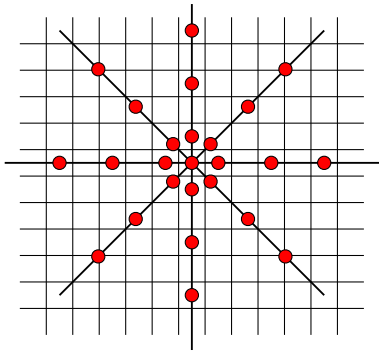

Figure 19: Sampling pattern of Fourier transform obtained from individual projections

Interpolate these values to a Cartesian grid isn't very straightforward, because every point carries an information about spatial frequency in original image and the inverse transformation is very sensitive to change in these values which strongly affect the resulting image. Therefore, it would be more comfortable to transform sampled values to another form. To get attenuation function $\mu(x, y)$ we have to inversely transform function $F(u, v)$

$$\mu(x, y) = \iint F(u, v) e^{2\pi i(ux+vy)} du dv \tag{22}$$

We try to express this integral in polar coordinates

$$du dv = \omega d\omega d\theta$$

$$\mu(x, y) = \int_0^{2\pi} \int_0^{\infty} F(\omega \cos\theta, \omega \sin\theta) e^{-2\pi i\omega(x\cos\theta + y\sin\theta)} \omega d\omega d\theta \tag{23}$$

Term $F(\omega \cos\theta, \omega \sin\theta)$ are just values of 2D FT along a line defined by angle θ, therefore guilt: $F(\omega \cos\theta, \omega \sin\theta) = Q_\theta(\omega)$.

$$\mu(x, y) = \int_0^{2\pi} \int_0^{\infty} Q_\theta(\omega) e^{-2\pi i\omega(x\cos\theta + y\sin\theta)} \omega d\omega d\theta \tag{24}$$

Here we can use fact that for parallel sampling geometry, a convenient symmetry property exists among the projection samples [19]

$$Q_{\theta+\pi}(\omega) = Q_\theta(-\omega)$$

$$\mu(x,y) = \int_0^\pi \left[\int_0^\infty |\omega| Q_\theta(\omega) e^{-2\pi i \omega p} d\omega \right]_{p=x\cos\theta+y\sin\theta} d\theta \tag{25}$$

What we see in square brackets is just inverse Fourier transform of transformed projections $Q_\theta(\omega)$ multiplied by absolute value $|\omega|$. In the spatial domain, it represents a projection filtered by a function whose frequency domain response is $|\omega|$, and is therefore called a filtered projection. This filtered function compensates the decrease in sampling rate displayed in figure 19 because gives higher priority to points further from center while repress the oversampled center. Situation is illustrated in following figure:

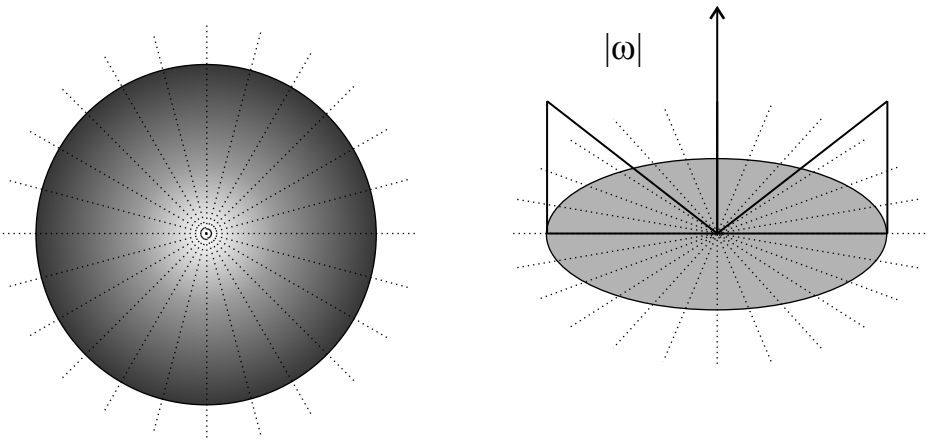

Figure 20: Influence of the weighting function $|\omega|$. Without it the image is oversampled in the middle but its presence in the integral ensures more balanced result

5.2 Example of image reconstruction

In order to describe process of reconstruction used in parallel beam tomography let's begin with simplified 2D model on an idealized monochromatic source and specimen that consists of two rectangles with different attenuation coefficients (figure 21).

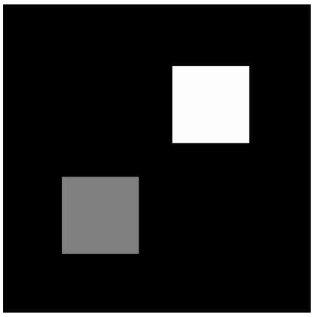

Figure 21: Idealized object of observation.The white square's coefficient is μ_1 and the grey square's coefficient is μ_2 . Dark part represents zero attenuation region. It can be imagined as two cubes inside low absorbing medium for example plastic and wooden cube inside polystyrene box

Object in figure above will be irradiated and we assume that the attenuation of radiation corresponds to a thickness. In other words, the squares consist of pixels and each pixel absorbs a little part of incoming intensity according to Lambert-Beer'law, as it is demonstrated in the following figure:

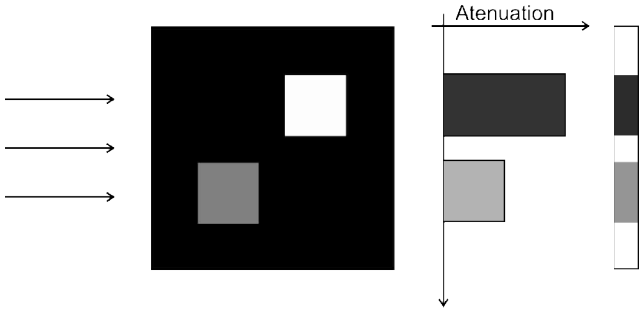

Figure 22: Attenuation of idealized objects. As we can see white square absorbs twice as much as the grey one

Since we have idealized homogeneous objects, the detected intensity distribution in figure above is inverse proportional to thickness of the object. Usually the obtained projections are converted to an inverse form (no attenuation is darker and attenuated are brighter). Otherwise the reconstructed image would be reversed. To obtain full object more scans under more angles have to be done. The set of these projections forms a complete Radon transform of the object. As they are put into matrix we obtain a *sinogram*. This process is described in following scheme:

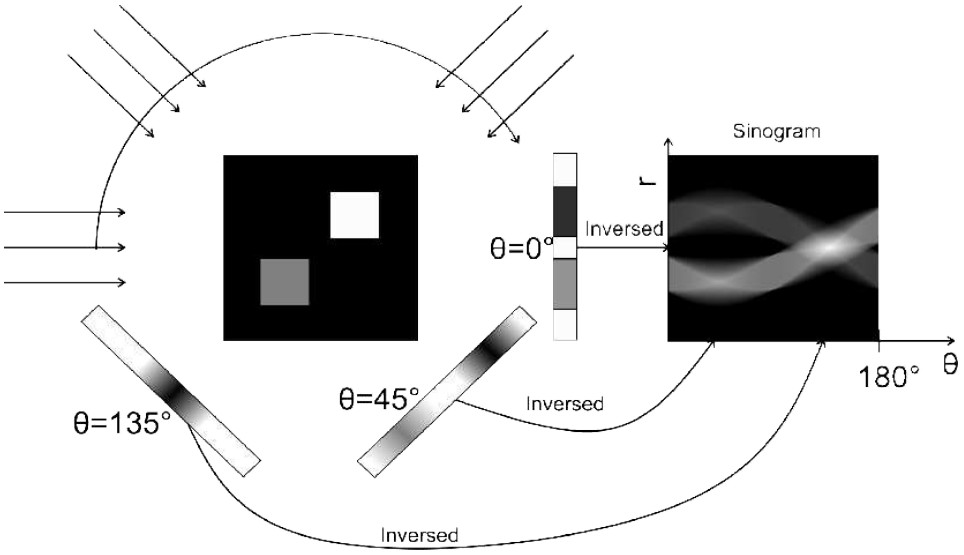

Figure 23: Single (inversed) projections are built together to form a sinogram

These projections are then Fourier transformed and using Fourier slice theorem we obtain a 2D Fourier transform (FT) of original object[10]. Then after inverse Fourier transform (IFT) we should get our 2 squares (figure 24). The quality of images depends on the number of single projection. Crescent number of projections improve the resulting quality.

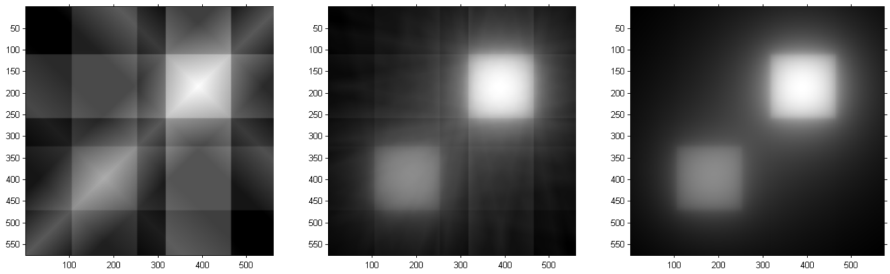

Figure 24: Unfiltered IFT (without using the weighting function $|\omega|$).The left image shows 9 projections around the object, each separated by 45 degrees. In the middle 36 projections are overlapped and on the right the image is obtained using 360 projections.

Reconstructions above are unfiltered without using the weighting function $|\omega|$ in inverse transform. When we apply it, the blurred edges and over gained centres of the squares disappear and the image gets sharp (figure 25).

[10]Reconstruction was computed in MATLAB with implemented algorithm

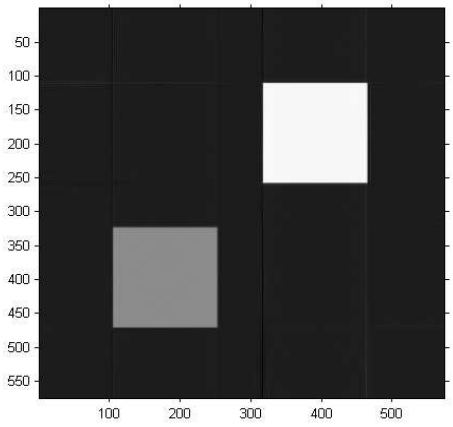

Figure 25: Filtered IFT reconstructed using 720 projections around the object

In this chapter we briefly described the process of image reconstruction from projections. We worked with quite simple parallel beam projection that can be relatively easily described. Although today machines use multiple fan beam sources enabling much faster and less invasive scans with higher resolution, the rough principle of reconstruction remains. There is a plenty of programs where the reconstruction algorithm is very well implemented (for example VG studio used in our laboratory).

6 Heat Transfer

Heat propagates from hot objects to cold ones. It is a consequence of entropy increase law. In general, we differ three ways how the heat can propagate[11]:

1. Conduction
2. Convection
3. Radiation

6.1 Conduction

Conduction can be interpreted as an energy transfer from more energetic particles to the less energetic ones due to interactions between them. It can be explained on a simple ideal gas model. The gas is kept in space between two walls that are maintained at different temperatures, creating a temperature gradient. "Hotter" particles are associated with higher energy while the "cold ones" with lower. When neighbouring particles collide, as they constantly do, a transfer of energy from the more energetic particles to the less energetic must occur. Temperature gradient causes that the energy transfer must occur in the direction of decreasing temperature.

The situation is much the same in liquids, although the molecules are more closely spaced and the molecular interactions are stronger and more frequent. Similarly, in a solid, conduction may be attributed to atomic activity in the form of lattice vibrations (called phonons). In an electrical non-conductor, the energy transfer is exclusively via these lattice waves, in a conductor, it is also due to the translational motion of the free electrons.

The mathematical theory of heat conduction was developed early in the nineteenth century by Joseph Fourier [20] .The theory was based on the results of experiments similar to that illustrated in figure 26 in which one side of a rectangular solid is held at temperature T_1, while the opposite side is held at a lower temperature, T_2. The other four sides are insulated so that heat can flow only in the x-direction.

[11] In fluids it is considered also a fourth type of propagation called advection. It is a transport of physical quantity (for example moisture or temperature) due to fluid medium motion

For a given material, it is found that the rate, q_x, at which heat (thermal energy) is transferred from the hot side to the cold side is proportional to the cross-sectional area A, across which the heat flows; the temperature difference, $T_1 - T_2$, and inversely proportional to the thickness, t, of the material. This can be expressed as[12]

$$q_x = -k\frac{A(T_2 - T_1)}{t} \tag{26}$$

Where constant of proportionality k represents a quantity called thermal conductivity, which is characteristic for the material. We can rewrite the equation 26 into differential form letting the thickness be dx and temperature difference dT. It is also convenient to divide it by area A.

$$\overline{q}_x = -k\frac{dT}{dx} \tag{27}$$

In this form we talk about heat flux that is defined as a rate of heat energy transferred through a given surface expressed in [W/m2].

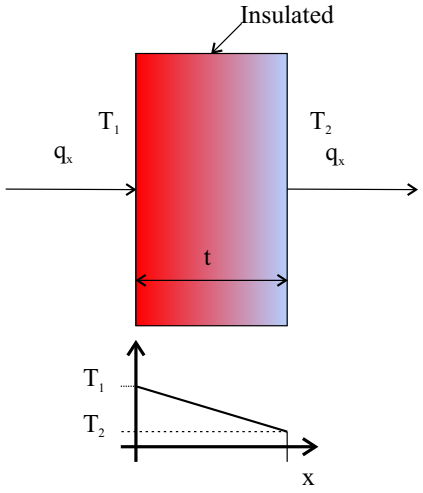

Figure 26: Heat transfer through an idealized rectangular object

In general, the heat flux is a vector quantity dependent on spatial coordinates[13].

$$\overline{q} = -k\left(\frac{\partial T}{\partial x} + \frac{\partial T}{\partial y} + \frac{\partial T}{\partial z}\right) = -k\nabla T \tag{28}$$

[12]it is convention to use minus sign by heat transfer rate to denote that heat flows from hotter to colder places

[13]Therefore the total derivative with respect to spatial coordinate, that is acceptable for one dimensional case, must be replaced by partial derivative

Here we assume that the heat flux doesn't depend on temperature [14] and the thermal conductivity k is equal for every direction.

6.1.1 Heat diffusion equation

Our goal is to set temperature distribution resulting from condition imposed on problem boundaries. Once this distribution is known, the conduction heat flux at any point in the medium or on its surface may be computed from Fourier's law. The temperature distribution could be then used to optimize the thickness of an insulating material as in our case by chamber design.

Suppose we want temperature distribution to become a function of 3D Cartesian system T(x,y,z). The equation can be derived by applying a thermal energy balance on a differential volume element in the solid (figure 27). Difference in heat transfer rate in and out of the element together with possible heat generation in element must be equal to heat accumulation within element.

$$q_{in} - q_{out} + Q_{generation} = Q_{accumulation} \tag{29}$$

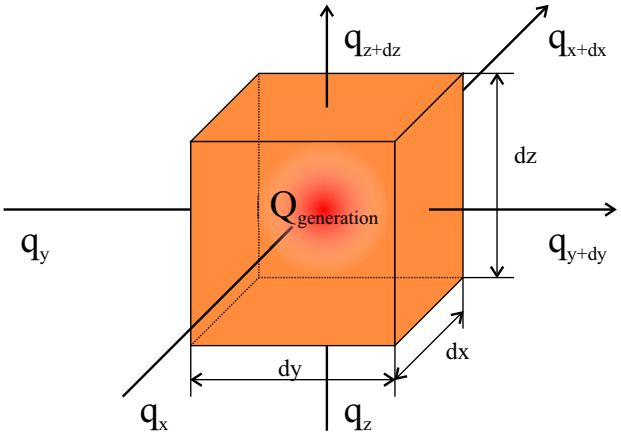

Figure 27: Illustration of a differential element of solid used for heat conduction equation derivation q_x, q_y, q_z fluxes through the walls and $Q_{generation}$ represents the heat generation inside element.

[14] This statement is in most cases acceptable, the temperature dependence is for most materials fairly weak and can be for higher accuracy approximated by linear dependence $k = a + bT$

The conduction heat transfer rate at the opposite surfaces can then be expressed as a Taylor series expansion[15]

$$q_{x+dx} = q_x + \frac{\partial q}{\partial x} dx \tag{30}$$

For simplicity we consider only heat transfer in x direction, other axes are analogical. So the difference between heat rates in and out can be expressed as

$$q_x - q_{x+dx} = -\frac{\partial q}{\partial x} dx \tag{31}$$

Here we could use identity from equation 27 but we have to notice that it works with heat flux which is heat transfer rate divided by area. Therefore to use equation 27 we have to multiply equation 31 by area, which in x diraction given as $dydz$.

$$\left(-\frac{\partial}{\partial x}\left(-k\frac{\partial T}{\partial x}\right) dx \right) dydz = \frac{\partial}{\partial x}\left(k\frac{\partial T}{\partial x}\right) dxdydz \tag{32}$$

For a homogenous material we could take thermal conductivity k outside the derivative and take it as a constant. Although in general it is a scalar function of spatial coordinates that relates to material distribution and cannot be neglected by derivation.

We also make a provision for a possible thermal source inside the element. In can reflect the situation that there is generated heat within the bulk as a consequence of external forces or the bulk contains radioactive material. Term associated with rate of energy generation can be expressed as

$$Q_{generation} = q_g dxdydz \tag{33}$$

Where q_g [W/m3] is the rate at which the heat is generated per unit volume $dxdydz$.The energy accumulation can be expressed as change of energy content in element volume per time

$$Q_{accumulation} = \rho c \frac{\partial T}{\partial x} dxdydz \tag{34}$$

Where ρ is density, c thermal capacity. The balance equation 29 divided by elemental volume $dxdydz$ come into following form:

$$\left(\frac{\partial}{\partial x}\left(k\frac{\partial T}{\partial x}\right) + \frac{\partial}{\partial y}\left(k\frac{\partial T}{\partial y}\right) + \frac{\partial}{\partial y}\left(k\frac{\partial T}{\partial y}\right) \right) + q_g = \rho c \frac{\partial T}{\partial x} \tag{35}$$

[15]Clearly the same is valid for other two coordinates, and we neglect higher order term

This equation, often referred to as the heat equation, provides the basic tool for heat conduction analysis. Its solutions, for prescribed boundary conditions, provide the temperature distribution in the medium.

6.2 Convection

Convection heat transfer involves two main mechanisms.The first mechanism is microscopical and is comprised of energy transfer due to random particle movement (diffusion).The second one is macroscopic and is related to the way how the particles move inside a fluid (meant air and liquid). This fluid motion (flow) is associated with the fact, that large numbers of molecules move collectively or as aggregates. Such motion, in the presence of a temperature gradient, contributes to heat transfer. Convection heat transfer may be classified according to the nature of the flow. We speak of forced convection when the flow is caused by external means, such as by a fan, a pump, or atmospheric winds (figure 28). As an example, I consider the use of a fan to provide forced convection air cooling of computer processor. In contrast, for free (or natural) convection, the flow is induced by buoyancy forces, which are due to density differences caused by temperature variations in the fluid. Convection cannot take place inside solid bodies because there is no significant diffusion of particles. However a solid-fluid interface represents the main heat transfer mechanism.

The convective heat flux q_c [Wm^{-2}] can be expressed similarly to the conductive heat flux.

$$q_c = h(T_S - T_\infty) \tag{36}$$

Where h [$\mathrm{Wm}^{-2}\mathrm{K}^{-1}$] represents so called convection heat transfer coefficient, which is lypical for every interface and depending on surface geometry, nature of fluid and many other factors. The choice of optimal h plays an important role for reasonable calculations because its values can vary from 1 to 250 for gas-solid interface and from 50 to 20000 for liquid-solid interface [21]. T_s stands for surface temperature while T_∞ for ambient temperature (room temperature).

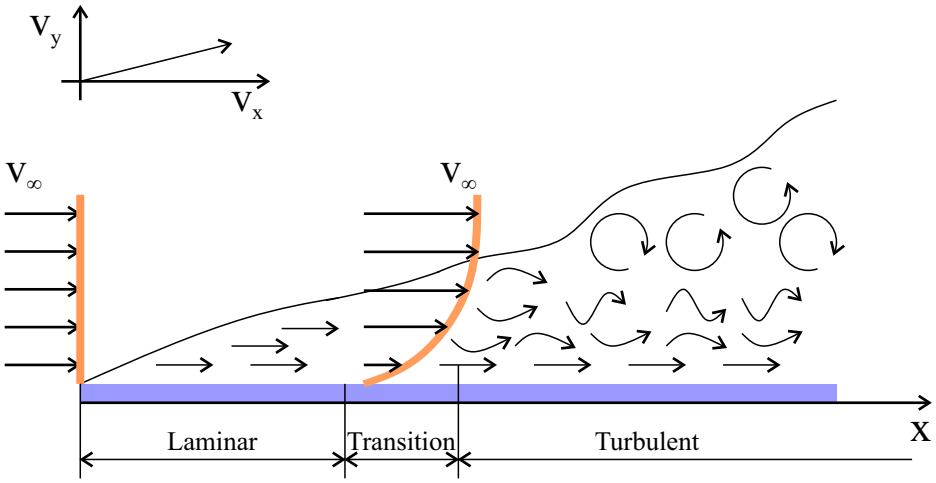

Figure 28: Schematic illustration of convection forced by air. Near the surface the laminar flow dominates and the velocity of particles is relative slow. Further from the surface turbulent flow also occurs as a consequence of air viscosity. Free convection would be illustrated very similarly but the figure should be vertical because the flow caused by buoyancy forces aims upwards.

7 Overview of available solutions for temperature controlled tomography

X-ray computed tomography is no doubt a wide spread technique non-destructive analysis however the fast industrial development nowadays requires besides high resolution measurements also observation of samples under various environmental conditions. One of the most required parameter is temperature. With increasing or with decreasing temperature material dilatation occur or shortening and that can cause possible in assembly dysfunction. These size changes can be hidden inside an assembly and therefore hard observable with usual methods like 3D optical scanning. Computed tomography can reveal this changes and compare it with CAD data.

7.1 cooling

The way of cooling or heating an objects depends mostly on their size.Very small objects (in size of millimetres) put much different demands on cooling and heating than large object (in size of tens of centimetres). There are special specimen stages for objects in range of millimetres capable to cool or heat the specimen during scan. There are even stages capable to compress or tensile the specimen 29 b.) . Some of them uses Peltier's cell like In-Situ peltier in figure 29 a.) . These stages are able to cool down specimen approximately 40 °C below the ambient temperature.

a.) b.)

Figure 29: a.) Heating and cooling stage for μCT from company *Bruker*. The peltier can decrease the temperature 40 °C below the ambient temperature and the heater can increase it up to 85 °C. Temperature is controlled using microprocessor unit within range 0.5 °C during the rotation. b.) Special specimen stage that can apply controlled compression and tension to an object.(source: https://www.bruker.com)

For some aplication the construction of the sample stages is relative easy and can be prepared for low costs [22]. However peltier stages for their constrained freezing power can be used to investigate samples requiring temperatures just slightly below zero like ice samples [23].Temperatures lower than $-40\,°C$ during scan aren't required only to proof thermal stability of industrial part. There are also samples where the low freezing temperatures are necessary. Biological samples often require temperatures far below zero to slow down biological processes [24], [25]. This low temperatures requires active cooling by liquid nitrogen ($-195.8\,°C$) or in extreme cases by liquid helium ($-269\,°C$). One way to achieve this is to use cryogenic stages developed originally for transmission microscopes and adjust it to the tube-detector constelation [26]. More advanced solutions can be found at the tomographic imaging facility at the BESSY electron storage ring [27] or at National center for X-ray tomography (NCXT) where the cryo-rotation stage was developed [28].

For a big objects a slightly different approach has to be chosen to control the temperature. One way to cool down a large parts is to use a liquid nitrogen's vapours like was done by Gerd Schneider at mentioned BESSY electron storage ring [29]. Another and in some cases much more available possibility is to use dry ice as a coolant on the bottom or top of well insulated and highly transparent chamber like was tested by Marian Kampschulte and his team in [30]. Enyu Guo with his colegues used dry ice by investigations of phase changes in ice cream [31].

7.2 heating

For heating of small objects can be used besides ordinary electrical heating also heating using laser beams. High energy lasers can be focused to very small spot giving rise to a huge local temperature increase [32].

On the other hand also heating of the specimen can be carried out variously depending on requied temperature and characteristics of the object. For example Manas Mukherjee by its tomography observations of aluminium foam used steel furnace with two relative X-ray transparent windows. The furnace was heated by halogen lamps with IR (infra red radiation) reflector and then slowly cooled by air [33]. For some investigations can be exploited ordinary medical CT with special specimen chamber.This was the case of Hiroshi Okabe and his team. They used special rubber furnace to observe fluid flow behaviour of heterogeneous rocks [34].

7.3 Our approach

Apart from these interesting and inspiring solutions the possibility of temperature control by investigation of large industrial parts is vastly limited. That was also the motivation to develop relative easy and affordable method that could help to provide CT scans in freezing temperatures. We were focused on $-40\,°C$ since it is the lowest temperature, which should an industial component withstand without loss of function acording to [35]. There is a broadly accepted criterion that standard temperature range for industrial parts varies from $-40\,°C$ to $80\,°C$ (sometime $100\,°C$). Therefore we wanted a solution for a stable repeatable $-40\,°C$ scans. Principe of the cooling of large samples was already indicated by Tomáš Koutecký in his work, where he tested first prototype chamber with special coolant boxes [36]. Meanwhile was manufactured a new redesigned type of chamber so the first step was:

- Testing of the new chamber and finding the optimal position of the coolant.

Besides we required the stable position of the sample for repeatable scans. Firs prototype of a sample holder was designed already by Markéta Tesařova. However her original design cannot be correctly printed on 3D printer so the flowing step was:

- Design of a sample holder that would fit into chamber and could be printed on 3D printer.

Test of the new chamber revealed its disability to hold stable temperature for a time required for a full scan (approx. 35 min) independent from position and amount of coolant. The transport of coolant and sample from freezer strongly affected the temperature progress and the coolant wasn't able to cool down the sample. We wanted to avoid the transport so we came with chamber that should be placed into freezer with sample already inside. Next goal was therefore:

- Design of a new chamber (supported by heat transfer simulations) that fits into freezer.

This approach seemed to be more successful because as the entire chamber with sample was cooled down to $-40\,°C$ the temperature inside the chamber stood still for more than half hour. However this chamber had smaller inner space and the sample holder cannot be used so the position of sample was fixed with two sponges. Next step we made:

- Comparison of scanned samples in VG studio and evaluation of changes due to temperature change.

Meanwhile we came with idea to build a chamber to test the opposite end of the industrial standard temperature range and namely 80 °C. So the additional step was:

- Construction of chamber capable to maintain stable 80 °C by preserving X-ray transparency.

Final step was:

- Comparison of scans at −40 °C 20 °C (room temperature) and at 80 °C

8 Cooling Chamber

In our project we focused on development of a chamber in which we would be able maintain $-40\,°C$ for a time necessary for a full CT scan. The required time can vary from 30 minutes to hour, depending on size and composition of observed sample. This project was based on a several experiments and measurements had been carried out by Tomáš Koutecký , and it helped us to find out where to continue.

8.1 First prototype chamber

First we worked with big polystyrene chamber designed by Tomáš Koutecký. Chamber was made from 2 parts,in the bottom is hole where should be placed a specimen with its holder . On top of the bottom part was space for coolant boxes. The second part had a bigger diameter and rectangular offset in the middle to lock on bottom part to form a relative airtight connection. Model of this chamber with base dimensions is in flowing figure:

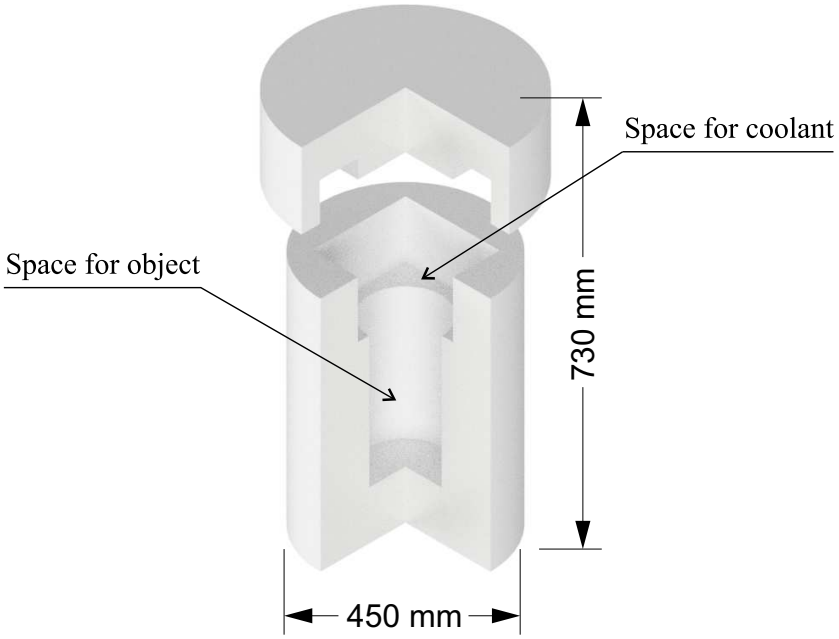

Figure 30: Model of polystyrene chamber. the diameter of botom is 450 mm and the inside space has diameter 190 mm and height 350 mm

8.1.1 The Coolant

The fist experiment had to reveal a necessary amount of coolant for keeping temperature on desired value for a relative long time. The coolant self was prepared by external chemical company. It was a mixture of water and monopolypropyleneglycol (propane-1,2-diol), this compound build a basis of almost every antifreeze. Concentration ratio here plays an crucial role because it determines the final freezing point of the mixture. This effect is also known as a freezing point depression[16]and occurs when two substances with different freezing points are mixed (it is very good observable on salted water that doesn't freeze at 0 °C). In general guilt that with increasing concentration of lower freezing point substance linearly decreases the freezing point of entire solution. When the substance melts, it means that it changes the state of matter and till isn't completely melted the temperature should stands still at freezing-melting point(figure 31). Just like an ice cube inside glass when it starts to melt slowly the temperature of melted ice (water) remains 0 °C till the ice isn't completely melted.

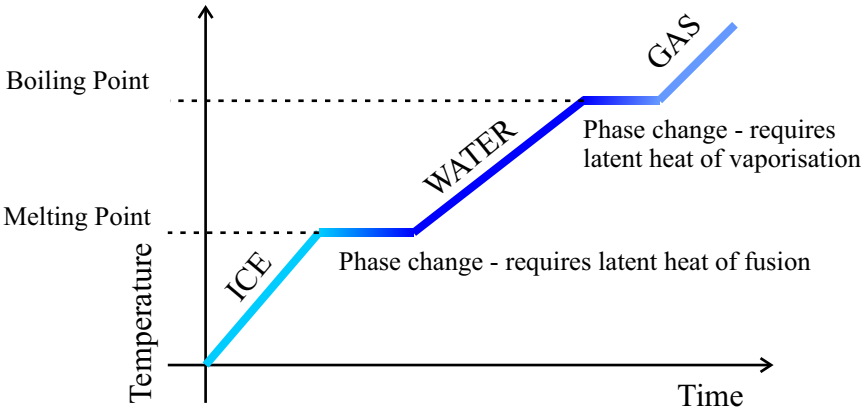

Figure 31: Idealised diagram of phase changes with increasing temperature and time

8.1.2 Boxes

The coolant was inside boxes with dimensions $175 \times 10 \times 40$ mm and every box has volume 500 ml. The fist issue was how to place these boxes inside the chamber to use maximum possible spaces. Second issue was how to carry them from refrigerator to chamber as fast as possible because every second in

[16]or melting point elevation when the boiling temperature of the mixture shifts to higher temperatures as a consequence of presence of another substance with different boiling point

ambient air can negatively affect the time till the temperature stabilize. To fulfil both requirements an aluminium box holder was made.It was capable to carry 5 boxes and was equipped with chain handlebars for easy manipulation during inserting and removing from chamber.

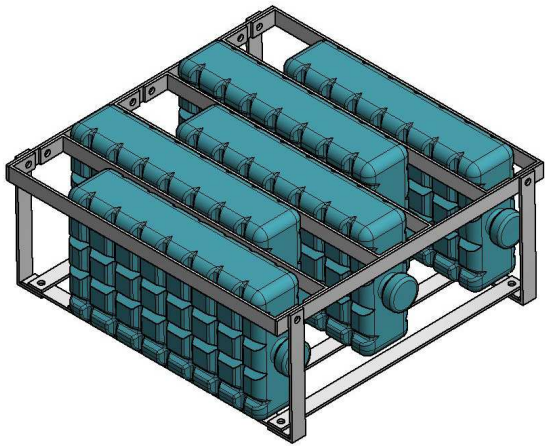

Figure 32: Boxes inside aluminium holder

8.1.3 Temperature measuring device

Progress of temperature was measured by ALMEMO 2590-4AS universal data-logger from company ahlborn. It was equipped with thermocouple ZA9020-FS with resolution 0.1 °C and range from -200 to 1370 °C

Figure 33: ALMEMO 2590-4AS universal data-logger, source:www.ahlborn.com

To attach thermocouple on our object of interest, thermal paste ARCTIC MX-2 was used. This paste is commonly used to guide heat from computer processors.

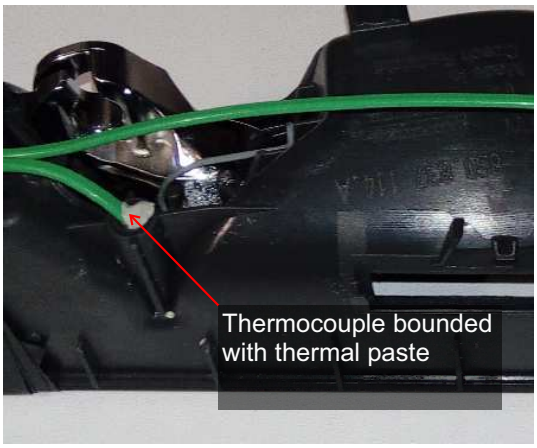

Figure 34: Thermocouple attached on car handle using thermal paste

8.1.4 Experimental measurements

Our object of interest(car handle) was placed inside chamber and immediately after that, there was inserted box holder with 5 boxes (together 2.5 l of coolant).The chamber was closed and the temperature progress was measured separately on coolant boxes and on handle.It can be seen on following figure.
On the first sight are obvious two thing. First that the coolant doesn't undergo a phase change so the temperature doesn't stand still and slowly rises with time.Second is that during time when the handle was in contact with ambient air rapidly increased its temperature. Naturally the air in the chamber before insertion was at 20 °C so it also affected the temperature progress. It lasted 40 minutes till it was cooled down but its temperature was still about 20 °C higher than temperature of coolant. We can see that nearly after one hour the temperature of boxes and the handle correlate in its progress but the temperature of handle is far above desired value.

First thing we tried to change was the amount of coolant. But the chamber had only space for 5 of them. The only way was to find a box that perfectly fits the space for coolant and fill it with it. We found a matching box with volume 4.5 litters.Although the space for coolant has dimensions $250 \times 250 \times 100$ mm and therefore 6.25 litres, this space cannot be completely exploited.

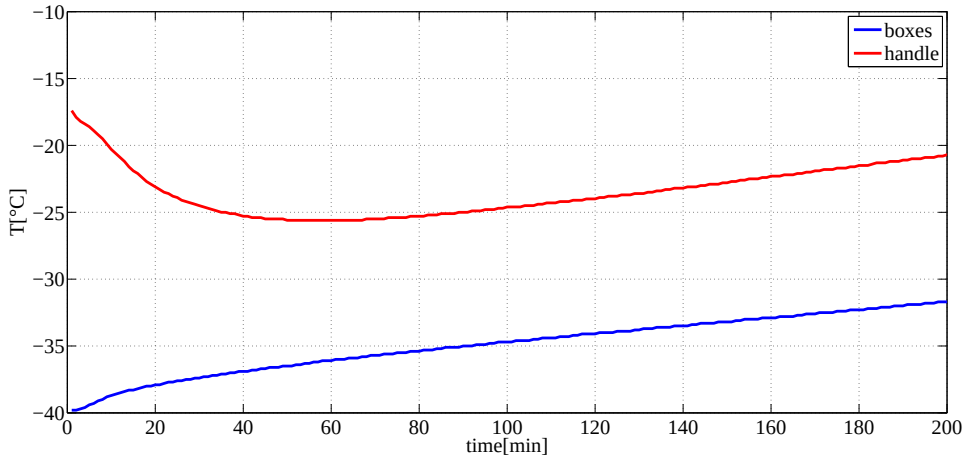

Figure 35: Progress of temperature during nearly 3 hour on car handle and boxes inside tested polystyrene chamber

The coolant must have its own box and there must be also a way to hide thermocouple. The box was filled with 4 litres of coolant and the measurement was carried out. The reason why the coolant doesn't undergo phase change was discovered. The concentration radio of water and monopropyleneglycol should ensure that the mixture freezes exactly at $-40\,°C$. Unfortunately the mixture doesn't freeze but change to a paste-like substance. As the temperature increases the paste is getting more diluted till completely changes to liquid, so the temperature continuance is more or less monotone.

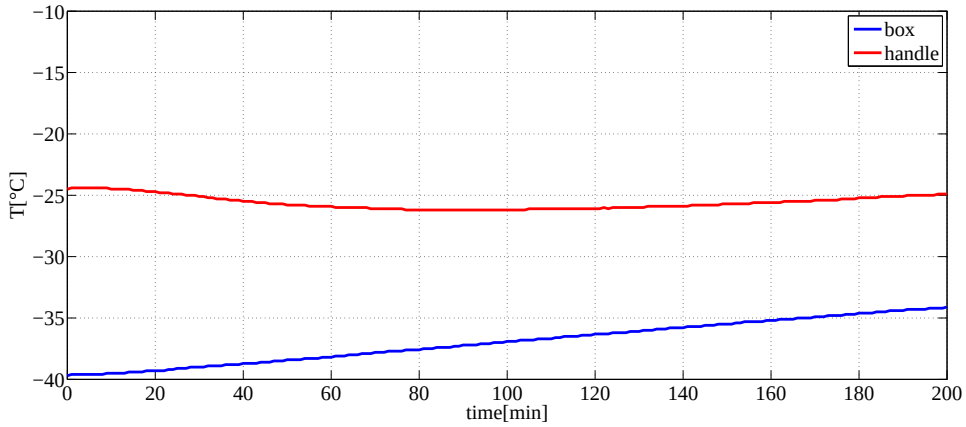

Figure 36: Temperature of car handle with 4l box of coolant in time. The temperature of the handle corresponds to temperature of inner air

The increase in temperature is slightly slower than in previous case due to bigger amount of coolant since more of the coolant means a higher thermal capacity. Although the temperature of handle follows the temperature of coolant its still about 10 degrees hotter than coolant. Short time period, during which the sample is in contact with ambient air obviously strongly affect the result. Need for faster sample transport from refrigerator to chamber but also a need for fixed position of sample inside chamber forced us to find a suitable sample holder that would fit into chamber.

8.1.5 Sample Holder

Design of sample holder for our chamber was already proposed earlier by Markéta Tesařova, who also design the chamber self. For the purpose of to

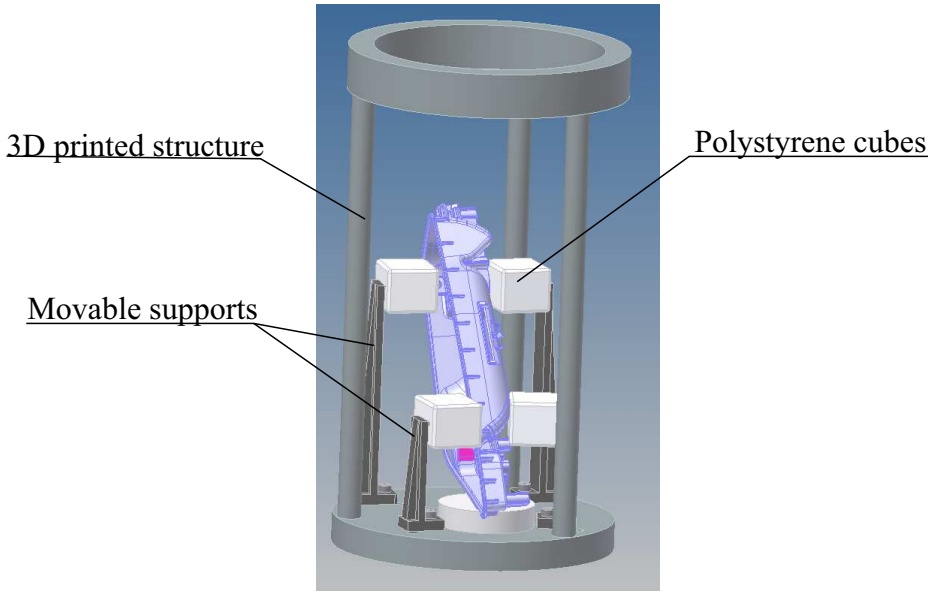

Figure 37: Original sample holder design by Markéta Tesařová.

manufacture this holder a little complication occurred.We had to redesign the movable holders because for 3D printer is much more easier when the part has got one flat site where it can start to print.We redesign them according to figure 38.

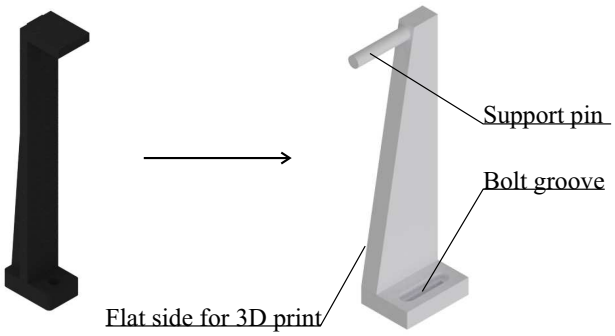

Figure 38: Design of new movable holder.

Complete holder was made on 3D printer and as a material was chosen ABS (acrylonitride-butadiene-styrene). We chosen ABS because is available and can be used in low temperatures and stay ductile (figure 39).The complete holder is displayed in figure 40.

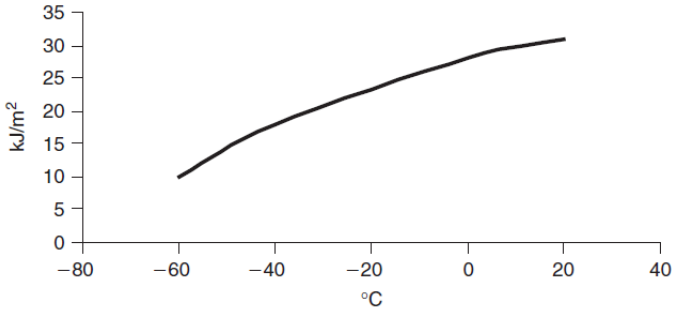

Figure 39: ABS: examples of notched impact strengths versus low temperatures, [37].

However even with the help of sample holder we cannot get rid of the negative heating caused by transport. We tried also a new coolant as a mixture of water and ethanol with 55% of ethanol that should depress freezing point of mixture down to $-40\,°C$. Unfortunately it didn't meet the expectations for higher cooling potential. The temperature progress using this type of coolant is in figure 41. Beside that we tried to insert smaller coolant boxes under the holder or even near the handle. Even that doesn't led to success and we had to find new solution.

Figure 40: Complete holder with car handle, without polystyrene supports on holders points

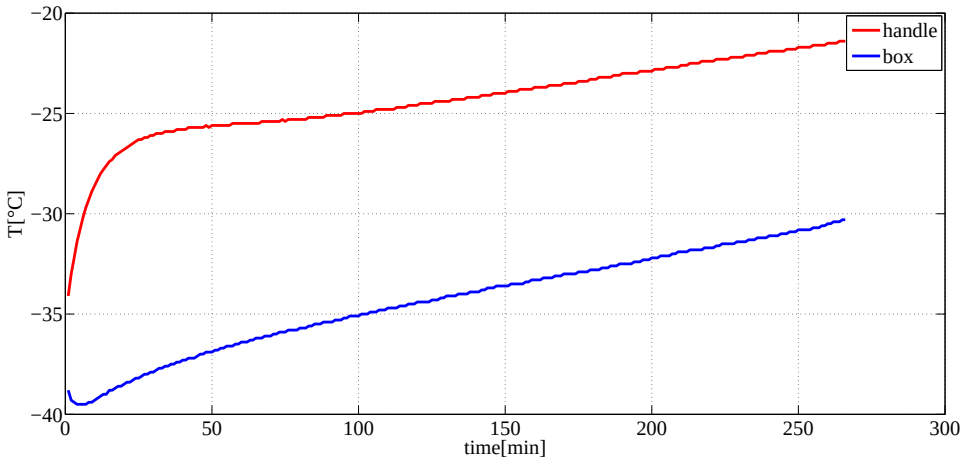

Figure 41: The temperature progress using water-ethanol mixture as a coolant.The progress is very similar to previous ones. The moment of sample and coolant transportation strongly affect the initial temperature and the box consequently cannot cool down the handle to desired temperature

Next idea was a dry ice in spite of fact that it sublimates by $-78\,°C$. The car handle was in holder and cooled down to exactly $-40\,°C$ then we moved it fast to chamber and covered it with boxes holder filled by dry ice pallets and closed. The temperature progress is in following figure.

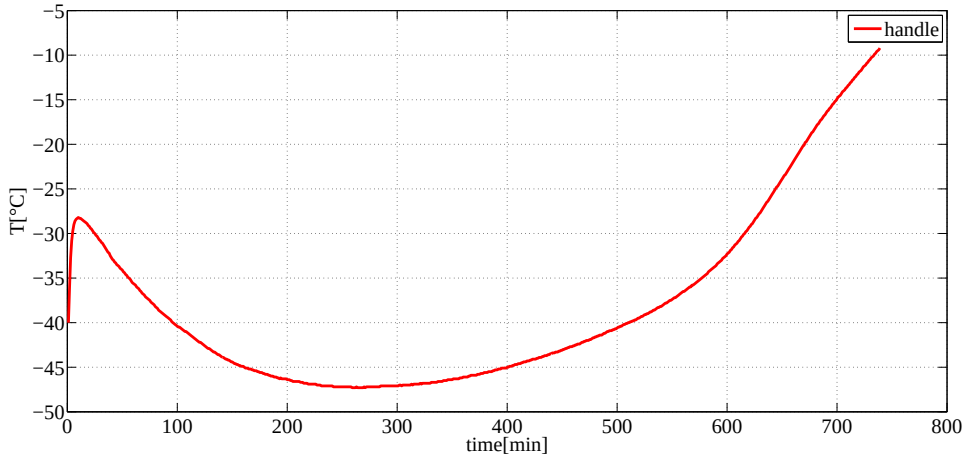

Figure 42: Temperature progress of car handle when the coolant is dry ice. We can see the fast temperature increase that is caused by transport and manipulation in ambient air

Dry ice show up as a very effective coolant that can last relative long but unfortunately for our purposes was too cold and we had to find another solution.

8.2 New version of chamber

Main idea was to prevent sample from contact with ambient air, so we proposed a similar polystyrene chamber but of smaller size that can fit into refrigerator. Before the final design we wanted to optimize the geometry of chamber with thermal analysis using FEM (finite method element). We used Inventor with plug-in NASTRAN where these calculations provided. Ilustration of used model is displayed in figure 43. Inventor has a huge database of materials with their mechanical and physical properties that was very useful by thermal conductivity (k) determination. More problematic was a convective heat transfer coeffitient (h) because its value strongly affect the result and cannot be exactly set. We used values from one study [38] where the value of convection coefficient for polystyrene-air surface varied from 17 to $21\,\mathrm{Wm^{-2}K^{-1}}$. We worked with the bigger value to make provision for the worse scenario. Final parameters of the simulation are in table 2.

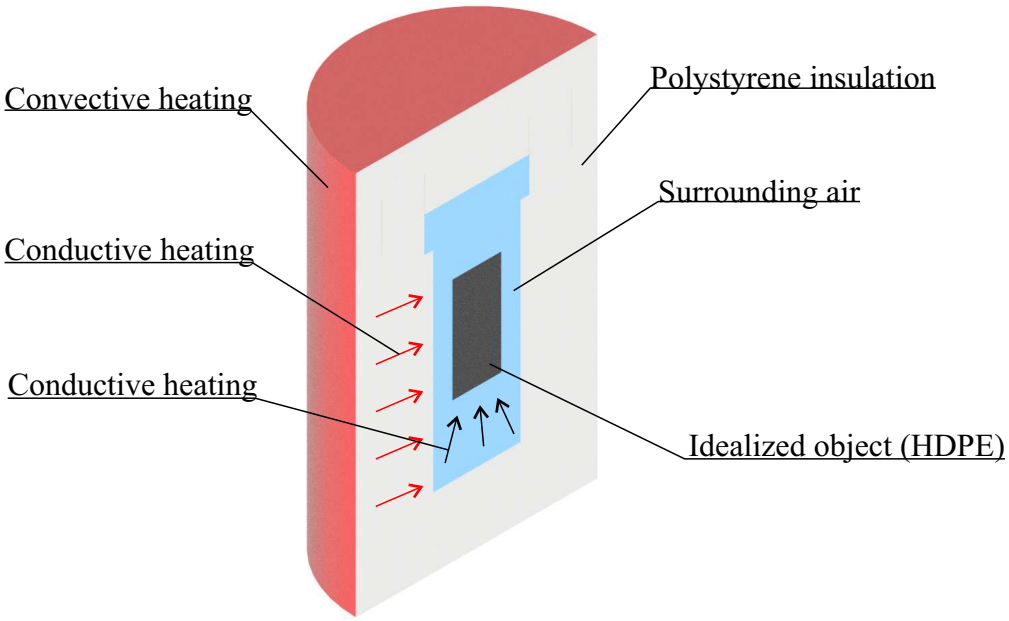

Figure 43: Model for FEM analysis. We assumed convective heating of chamber surface and conductive heat transport within polystyrene. Since the air in the chamber is closed, there cannot arise significant air flow so only conductive heat transport was assumed and convection was neglected

Table 2: Parameters of FEM analysis

air density	$1.20\,\mathrm{kgm^{-3}}$
air thermal capacity	$1.20\,\mathrm{Jkg^{-1}K^{-1}}$
air thermal conductivity	$0.025\,\mathrm{Wm^{-1}K^{-1}}$
polystyrene density	$30\,\mathrm{kgm^{-3}}$
polystyrene thermal capacity	$1210\,\mathrm{Jkg^{-1}K^{-1}}$
polystyrene thermal conductivity	$0.037\,\mathrm{Wm^{-1}K^{-1}}$
polystyrene-air convection coefficient	$21\,\mathrm{Wm^{-2}K^{-1}}$
HDPE density	$952\,\mathrm{kgm^{-3}}$
HDPE thermal capacity	$2859\,\mathrm{Jkg^{-1}K^{-1}}$
HDPE thermal conductivity	$0.211\,\mathrm{Wm^{-1}K^{-1}}$

Different geometries of chambers were involved into test. One had relative thin wall and big inner space another stronger walls and smaller inner space. The goal was to compare different geometries to choose the optimal one. The change of parameters with temperature wasn't involved[17]. We calculated transient heat transfer from chamber surface to object in 10 time steps where every lasted 720 s.

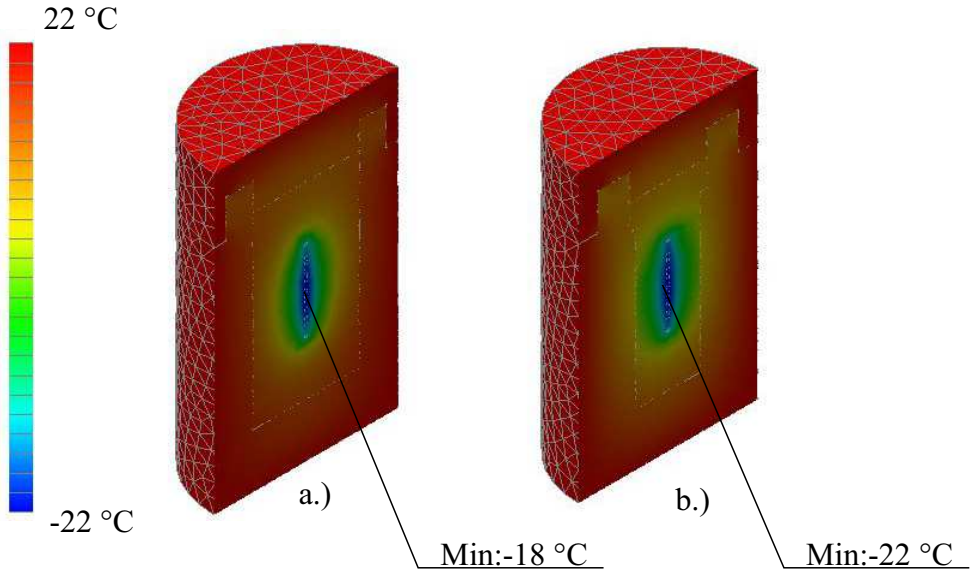

Figure 44: Comparison of heat transfer simulation for two models of chambers. We can see that the chamber with thicker walls keep the sample colder. The output is thermal distribution after 7200 seconds (2 hours)

After comparison we have chosen optimal dimension for a new chamber and sent the drawings (which are also included as addition to this work) to manufacturer. In the figure 45 is displayed model of the new chamber. There also left space for coolant but much smaller 150x150x50 mm that equals to 1.125 l but in fact there fitted only two 0.25 l boxes of coolant. The first experiment revealed much better results as the entire chamber and also a inner air were cooled down (figure 46).However our demand was a stable temperature for at least 35 minutes including preparations. Small amount of coolant in top space doesn't made this time significantly longer and we had to use plastic bag filled with coolant in vicinity of the sample.

[17]for example heat transfer or convective coefficient slightly changes with temperature

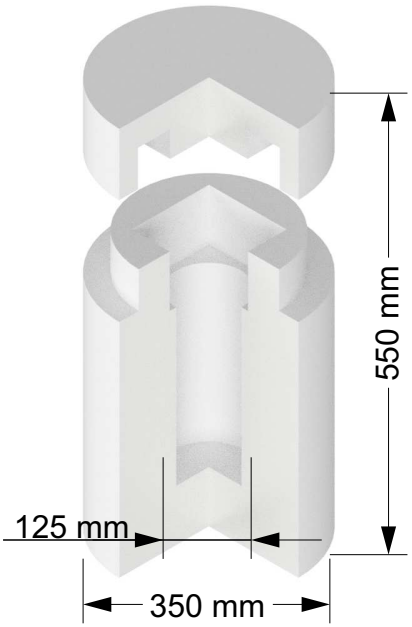

Figure 45: Model of smaller chamber that fits into refrigerator

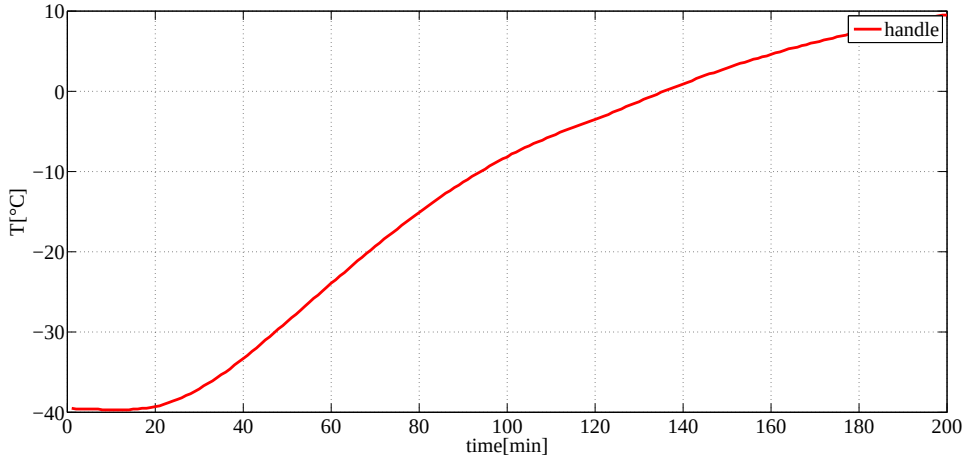

Figure 46: Temperature progress of car handle inside smaller chamber. The entire chamber with handle was taken out of refrigerator at $-40\,°C$. We can see that the temperature stand still nearly 20 minutes and then start to rise. The measurement was without any coolant inside

Since this chamber had another dimensions than the previous one we needed a new sample holder that would fit into this new chamber. Making smaller previous holder (40) wasn't possible because of much smaller diameter of inter space. The movable holders wouldn't be able to move. We used therefore 2 sponges and put the handle inside them as a sandwich. It also solved the problem with the short lasting stable temperature.Besides we used coolant bags that were filled with coolant and were wrapped around the handle and surrounded by two sponges. This solution worked well and the temperature stood still nearly one hour. Unfortunately it wasn't very optimal for CT scan because the coolant liquid attenuated the X-ray and the reconstruction would be then much complicated and the quality of the image would be in final lower. So we came with solution where the region of interest[18] on our handle is wrapped with two sponges and the rest is wrapped by coolant bags and this whole system is put into chamber. On the top is another sponge that serve as a air insulator. This way prepared chamber can withstand 50 minutes in 20 °C air and temperature change of handle is within 2 °C.

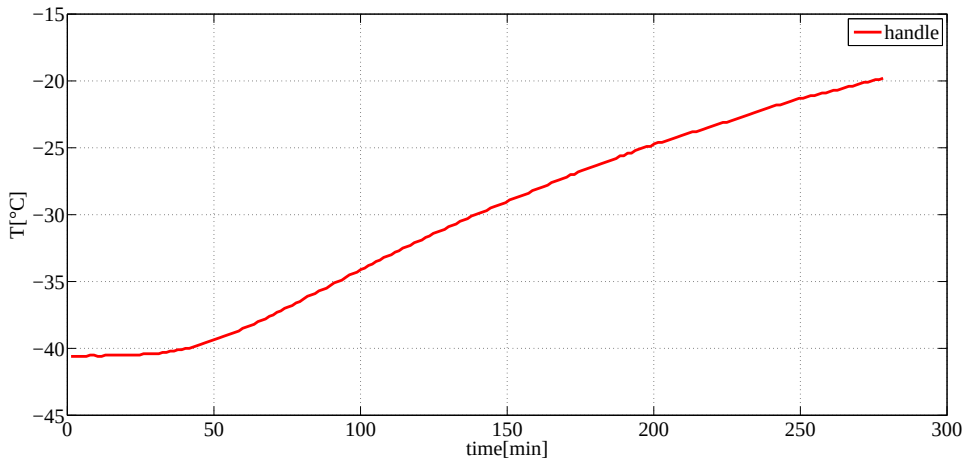

Figure 47: Temperature of handle during time. Fixed by sponges and half of the handle was wrapped in coolant bags

[18]In our case it was a metal spring that is responsible for proper handle movement and pulls the handle to previous position

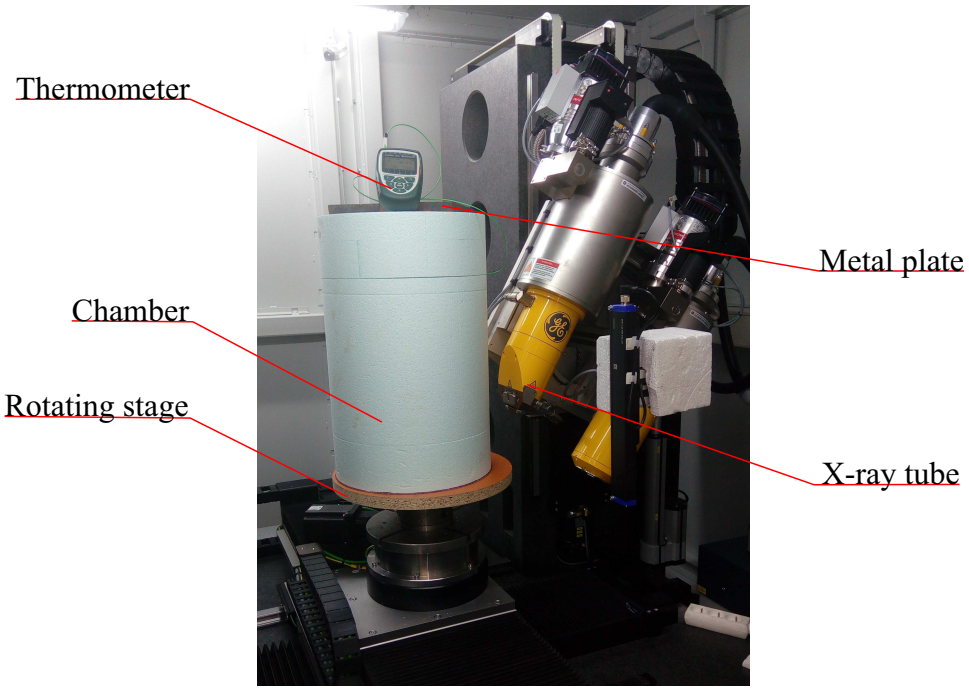

Figure 48: Photo of cooing chamber inside tomograph. Temperature is being measured also during the scan. The heavy metal plate fixes the chamber in stable position during rotation

8.3 Active dry ice cooling

Although the small chamber worked we wanted to create active full regulated cooling. In freezers are used compressor with thermal exchangers. This approach isn't optimised to as low temperatures as we desired. On the other hand there are manufacturers that are able to build compressor units capable to reach desired $-40\,°C$ but are too expansive and require large space, so this way was dismissed.

There is also possibility to use peltiers cell but as was mentioned in overview the peltier can cool down maximally to temperature $40\,°C$ lower than the ambient temperature. That means, when we would like to reach $-40\,°C$, the entire CT machine should operated maximally at $0\,°C$ which is impossible.

As we have seen in figure 42 the dry ice can be very effective but its temperature is nearly twice as lower as desired ($-78\,°C$). However if we could affect the amount of its vapour in the chamber we could control the temperature inside. That idea made us think of a system that could regulate the cooling power of dry ice.We came up with insulated tube equipped with regulating fan. Scheme of this tube can be seen in figure 49.

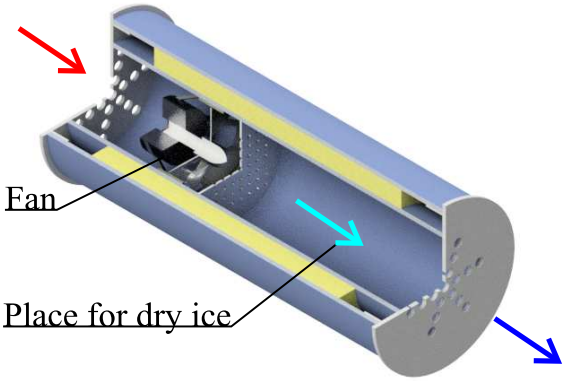

Figure 49: Scheme of cooling tube using dry ice as a coolant. The expectation was that the fan sucks the ambient air and blows it trough the dry ice making it cooler. Flowingly the cool air enters the chamber leading to temperature decrease. The rotation of fan can be regulated to set a optimal air flow.

The cooler was mounted on the top of the small chamber and the vacancy was filled with thermal insulation. The complete cooling tube mounted on chamber can be seen in figure 50 .

Unfortunately this solution doesn't fulfilled the expectations putted on it. Independent from the fan speed the temperature in chamber still increased. When the airflow was too fast the air doesn't cool down enough so relatively warm air was blown into chamber. On the other hand when the speed of the fan was too low the ice dry vapours escaped also trough the top of the tube. We also tried to put foam insulation between the output and the ice to slow down the air right before chamber input but it wont help. Unfortunately this solution had to be dismissed.

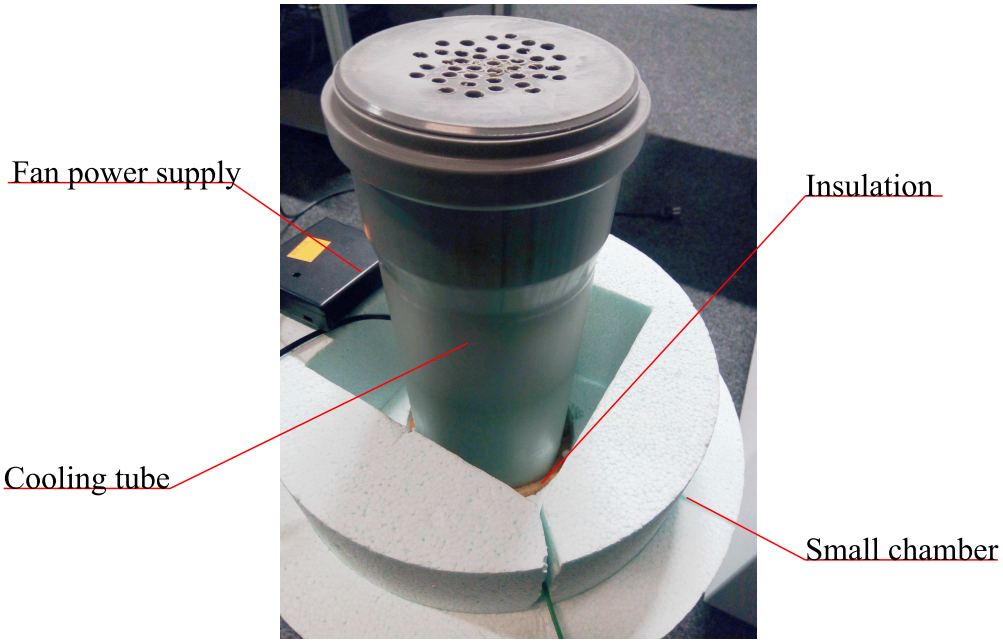

Figure 50: Cooling tube mounted on the top of small chamber. The vacancy is is filled by insulation.

9 Heating chamber

Manufacturers that produce various mechanical parts and devices require often their thermal stability not only for temperatures below 0 °C but also for temperatures relative far above room temperature. That was the motivation to construct besides cooling chamber also chamber where we would be able to reach at least 80 °C without affecting the X-ray transparency and image quality.

9.1 Material

Relative high temperature resistance and high X-ray transparency strongly restrict the pallet of usable materials. Expanded polystyrene that was used in case of cooling chamber is perfect material for building models and has very good insulation properties but doesn't withstand temperatures above 85 °C and become soft. We inspired our self by design of refrigerators. Their case is built from 2 thin metal plates that are separates few cm and the vacancy is filled by polyurethane foam. This way made wall show a very good insulation properties by maintaining stiffness and durability necessary to build cases. Naturally the metal plates had to be replaces by something less x-ray absorbing. We decided to use fibreglass laminate because is relative transparent for X-rays and has satisfying thermo-mechanical properties. This composite material can be very durable and relative ductile and can be moulded to various shapes. Besides can easily withstand temperatures above 100 °C[19].

9.2 Heating source

Heating is in respect of technical requirements, much more simpler than cooling. To cool something, lots of equipment is needed, like compressors, thermal exchangers, pipes, special coolants and so on. To heat something (briefly speaking) is sufficient just a piece of resistant wire and electric current. Of course when it comes to heating with regulation and maintaining stable temperature inside closed chamber things are going more complicate. We used a heating spiral and connected it to electric current trough triac regulator soldered manually.

[19]Its glass transition temperature is at least 150 °C depending on type of resin

9.3 First prototype

We made our first prototype of heating chamber only to test if proposed design that involves fibreglass laminate and heating spiral, can fulfil all requirements putted on it. We used PVC plumbing pipes of diameters 20 and 10 cm as a form for laminate. We used 2 compound epoxy resin and regular fibreglass. The fibreglass was painted with resin and wrapped around the pipes[20] to form cylindrical shells after hardening. After the laminate become harder , the smaller shell was inserted into bigger one, and the vacancy was filled with polyurethane foam. This structure was then closed by two PVC covers that belong to typical plumber equipment. On the bottom cover was mounted the heating spiral. The spiral had to be insulated from joint with bottom cover. The scheme of this prototype chamber can be seen in following figure.

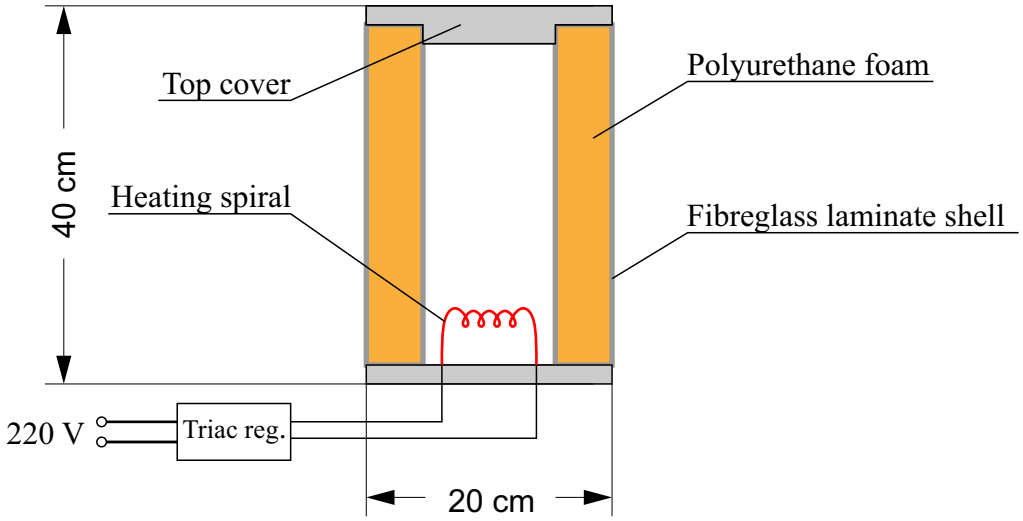

Figure 51: Scheme of prototype of heating chamber. the spiral was fed from electrical network trough triac regulator to control the heating power. Laminate can withstand temperatures 100 °C above but near the spiral were much higher temperatures so there cannot occur any contact. The same quilt for PVC

This chamber worked very well. With triac regulator we were able to control the heating power and therefore control the inner temperature. We tried to maintain the heat balance when the out coming heat would be compensated by heat generation by spiral but there were huge heat leak trough covers since their weren't insulated.

[20]pipes were covered by lubricant to easily remove the laminate

However the spiral was powerful enough to reach 100 °C but then occur problem with PVC since it shouldn't be used in temperatures above 80 °C for a long time because it become soft. Besides there was also a problem with strongly chemical stench caused by heating the relative fresh hardened epoxy resin. In spite of these inconveniences the prototype worked well and was also X-ray transparent which was proved by short CT scan. The part inside chamber was after a while of processing clearly visible. This motivated us to make a new better chamber with independent thermal regulation controlled by thermostat.

9.4 Second prototype

After experiences with first prototype we made a second one. We also used fibreglass laminate for cylindrical shells but this time with bigger diameter and height. We used handmade cylindrical forms made from bended steel plate. Also the spiral was different, taken from fan heater and capable to produce 2000 W. The covers were made from aluminium plate and insulated with polyurethane foam. The scheme of chamber is displayed in figure 52.

9.4.1 Thermal control

The heating spiral had enough power to heat the chamber in a short time period but there was a need to control the temperature. For this purpose we made a thermostat with changeable hysteresis equipped with durable thermocouple to control temperature. The thermostat with all his components was bought and soldered according to manual. But as a additional part we decided to control the heating power with triac regulator like in previous case. Because when the thermostat would switch on the spiral on full power the temperature would rise very rapidly and the thermocouple would immediately send signal to thermostat to switch off. This process could then lead to unwanted circuit fluctuation. With the regulator can be the heating power controlled to avoid these fast switch ons and offs.

Previous prototype also suffered on chemical stench caused by insufficiently hardened resin. We get rid of this inconvenience by drying the chamber in warm air for whole day. Besides we painted the whole chamber with heatproof paint to prevent the evaporation of resin but also to make the surface uniform (figure 55). First test of this way prepared chamber equipped with controlled heating spiral revealed its capability to maintain set temperature within range of 1 °C as we can see in figure 54.

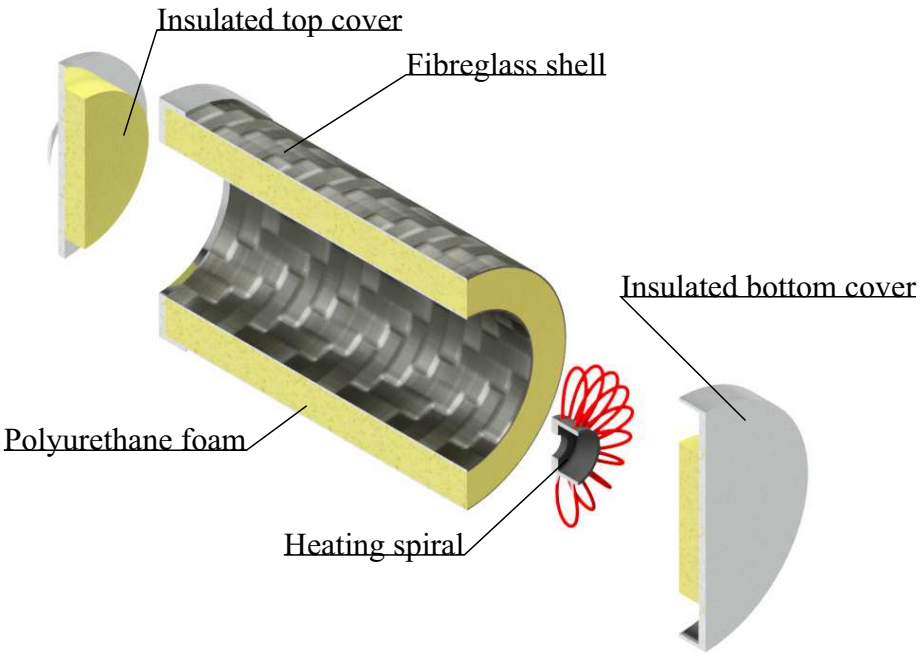

Figure 52: Scheme of final prototype of heating chamber.The inner diameter is 20 cm and the outer 30 cm, height of the chamber is 45 cm.The bottom cover contains cable connections for spiral power supply and thermocouple connector

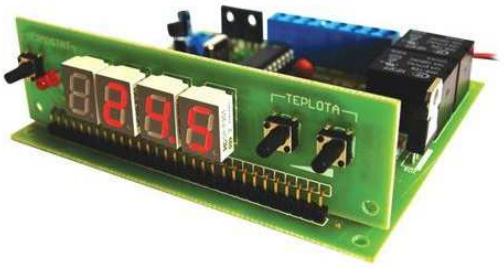

Figure 53: Hand soldered thermostat kit used for thermal regulation. Source: http://www.stavebnice.postreh.com/select.php?link=PT018

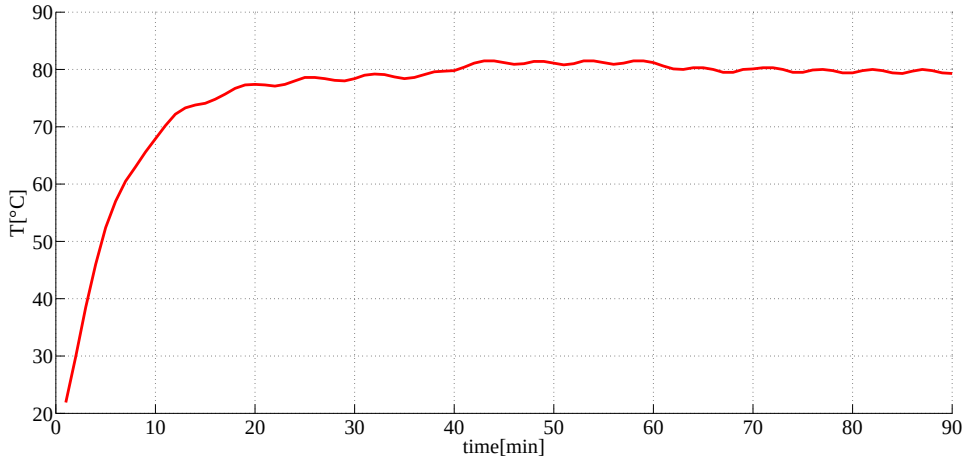

Figure 54: Temperature in heating chamber vs time. The thermostat was set on 80 °C and as soon as the temperature reached this value it began to oscillate around it. The hysteresis was set on 3 °C but the air in chamber has its own thermal inertia so there is a certain delay between the moment when the spiral heats and the detection of thermal change

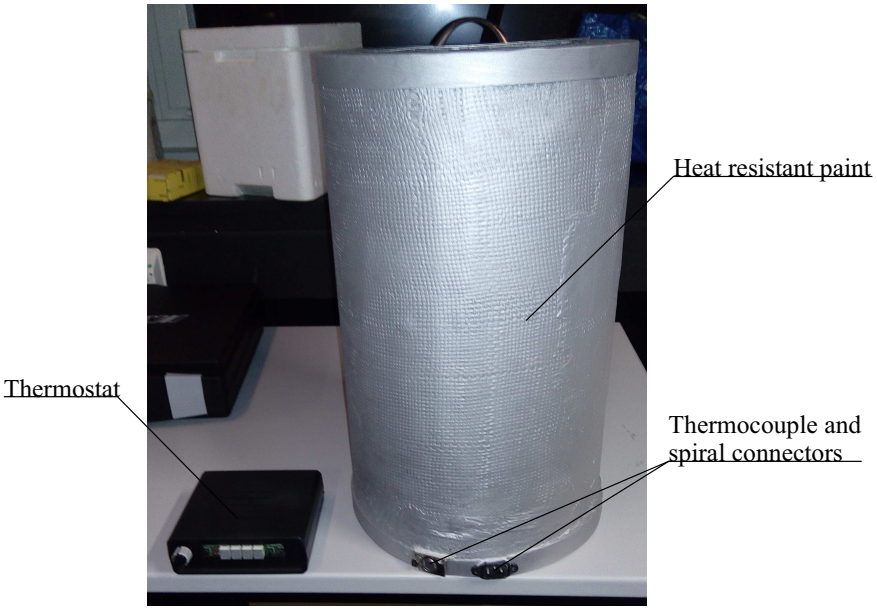

Figure 55: Photo of heating chamber with thermostat

10 Comparison of scans

10.1 Room temperature vs −40 °C

As the complete scans at−40 °C and at 20 °C were carried out we proceeded with comparison in volume graphic software *VG studio*. At this point I would like to thank again for helpful attitude to Michal Petrilak and Martin Kareš. Their help by chamber positioning, scans complementation and comparison was very valuable to me.

At first, we scanned the chamber at −40 °C. Then, at the second time, we scanned the same chamber at 20 °C. The chamber stood meanwhile in corner of acclimatized CT room to heat up to room temperature (Temperature progress for both cases can be seen in figure 56) .The parameters of scan were set according to previous experiments by Tomáš Koutecký [36]. Since we used also expanded polystyrene of different thickness.

Table 3: **Parameters of scans**

Acceleration Voltage	170 kV
Beam current	200 μA
Filters	Sn 0.1 mm, Cu 0.3 mm
Number of projections	2200
Exposure time	300 ms
Image averaging	2
Scanning time	35 min
Voxel size	50.025 μV

Before the scan, an alignment of the chamber had to be done, not only because the cooling chamber was of smaller diameter than the previous one, so the X-ray tube distance was shorter, but mainly to find optimal position of region of interest of our car handle. When we found the optimal position of chamber, we marked it by red marker on stage and on chamber. After that, the chamber was kept for one day in freezer at −40 °C. When the chamber was completely cooled to desired temperature, we proceeded to scan with pre-set parameters in relative fast manner to avoid heating by transport. The obtained data revealed certain inconvenience. The material of sponges, which were responsible for handle fixation, had similar attenuation coefficient as the main handle material. This fact had led to complication by exact surface determination of the handle. Because these materials could not be sharply separated.

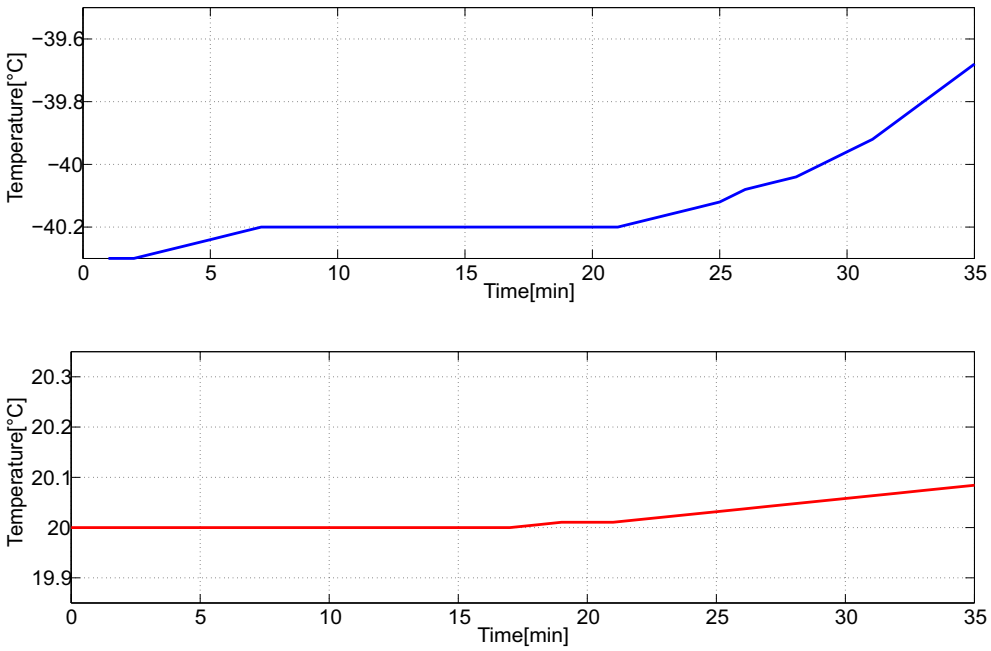

Figure 56: Temperature progress during scans. Each scan lasted for approximately 32 minutes. On the top it is the temperature evolution of handle at freezing temperatures and in the bottom at room temperature.

The surface determination is essential for comparison with another data. The complete dataset is made of voxels (volume pixels) and we need to create a sharp defined surface of observed object from them. As we have surfaces of both datasets, we can superimpose them and determine the magnitude of shape changes. However, due to the similarity of the attenuation coefficient of sponges and the handle, the calculated surface involves also parts that doesn't belong to handle and must be removed manually (figure 57). This process involves creating of volumes that doesn't involve the surface of handle but parts of sponges and excluding them from surface calculation. The shape of the handle cannot be restored perfectly but the main regions of interest were corrected very precisely and most of them weren't even affected by this inconvenience since they weren't in contact with sponges.

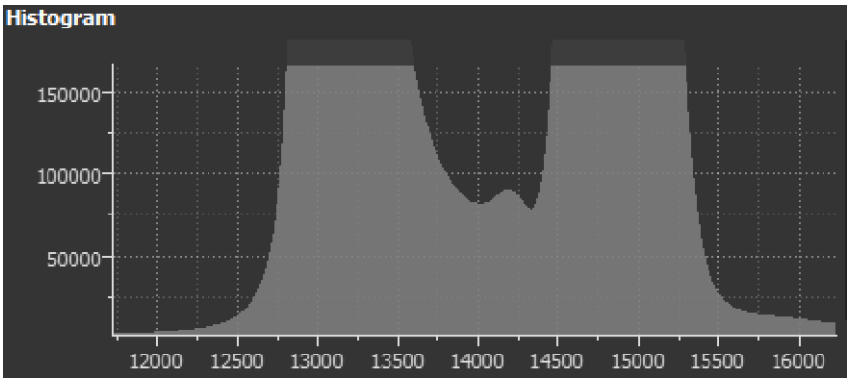

Figure 57: Histogram of scan obtained at −40 °C. Similar histogram of scan was also obtained at 20 °C since they differ only in temperature. The high peaks on the left and right are the attenuation peaks of the main materials of the handle. The little peak between them represents the surrounding sponge. As we tried to determine the border between handle and surrounding material to calculate sharp surface, this peak made it more complicated. Once we set the threshold before the peak we could neglect the parts of the handle but then when we moved the threshold further also parts of sponge were involved into final surface

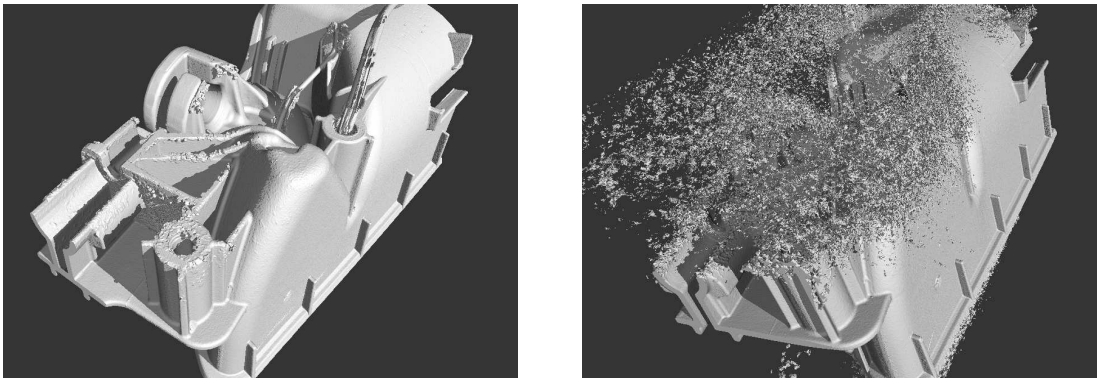

Figure 58: Surface fragments caused by sponge on the right. Cleared surface by excluding these fragments from surface calculation on the left.

Main region of interest was part of the handle where the handle self is connected to the body of handle. There are relatively tight contacts of different materials like in following figure.

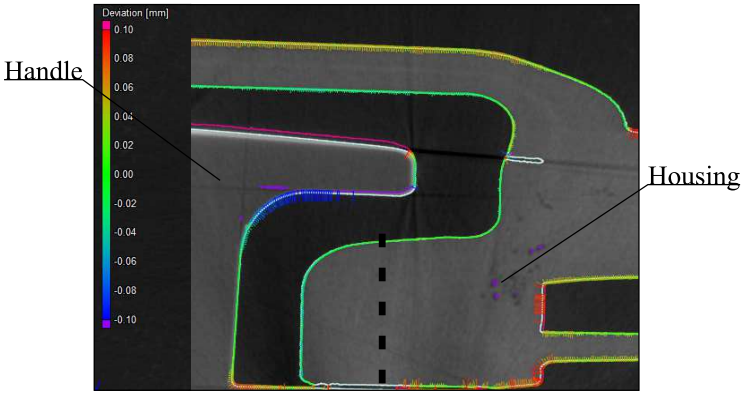

Figure 59: Comparison of surfaces of two scans obtained in different temperatures. As a reference surface the scan at 20 °C is taken and the scan at −40 °C is compared to it. The colour indicates the shift rate. The dashed line represents the rotation axis of the handle by opening. We can see that the part of the handle about axis at −40 °C is relatively deformed with respect to the same part at 20 °C. This result was already observed by Tomáš Koutecký

Before the observed shift in figure 59 we noticed also a surface mismatch on the handle itself. Namely, the handle was chromed and the surface tension due to thermal change slightly crinkled the chrome layer. It was observable in figure 60 but also by naked eye in figure 61.

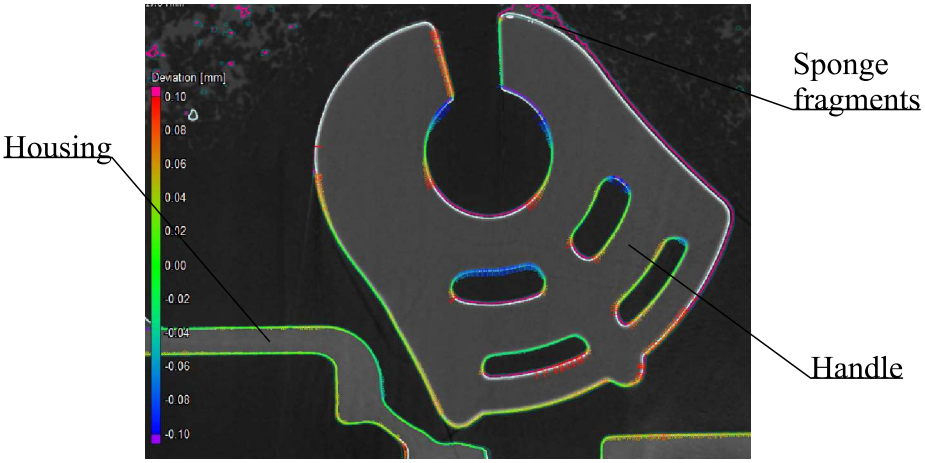

Figure 60: Comparison of bottom part of chromed handle.We can notice the unwanted fragments caused by sponges. They were removed near the surface not to affect the surface comparison. We can also see how the chrome layer gently crinkles the surface of handle

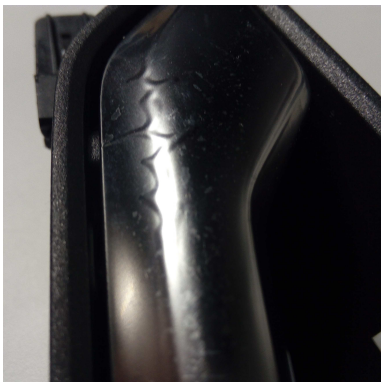

Figure 61: Separated chrome layer from handle as a consequence of often thermal changes

Little shift occurred also on ribs of the plastic housing. The entire housing of the handle acted as a membrane that inflated and deflated as the temperature changed. This fact caused that the tops of the reinforcing ribs were moving from to each other in a microscopic scale.

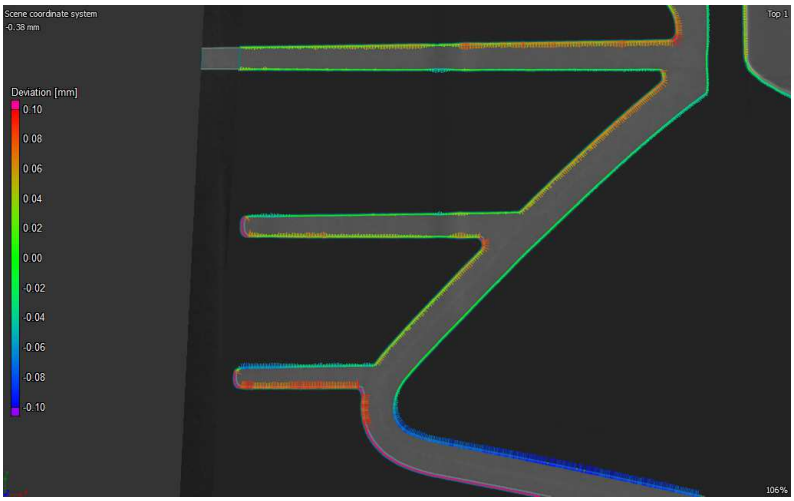

Figure 62: Plastic ribs of the housing are slightly shifted. By the reference scan at 20 °C the housing is slightly expanded and the tops of the ribs are little further from each other than at −40 °C

10.2 Room temperature vs 80 °C

Firstly, the positioning of the handle inside the heating chamber made us problems as the sample holder couldn't withstand this high temperature. Even through the handle was kept at 80 °C, the spiral was kept at nearly 120 °C so the bottom of holder started to melt. Therefore the handle had to be glued to inner walls of the chamber and being scanned in skewed position relative to scanner as it is demonstrated in the following scheme:

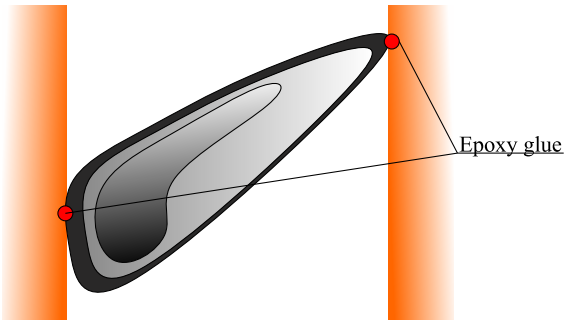

Figure 63: Illustration of car handle being glued to inner walls of chamber

During the scan i was important to watch the position of the cables that were connected with the chamber. As the entire chamber rotated the cables (power cable and thermocouple data cable) were slowly coiling up around the stage. If they stuck it could move the chamber and the entire scan would be useless. So we cleared the way for the cables and glued the chamber to the stage (figure 64).

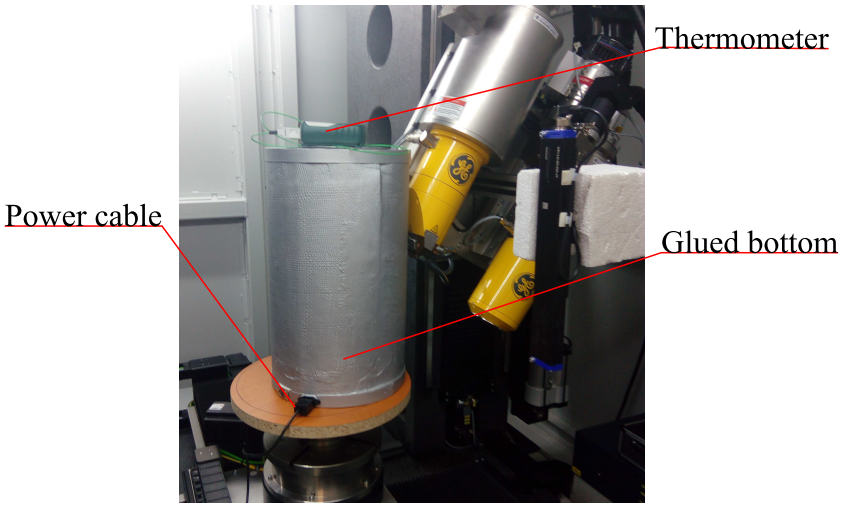

Figure 64: Heating chamber into CT scanner

Since the handle wasn't surrounded by any material but air the final reconstruction was much clearer than the previous ones at lower temperatures, the final model was sharper (figure 65).

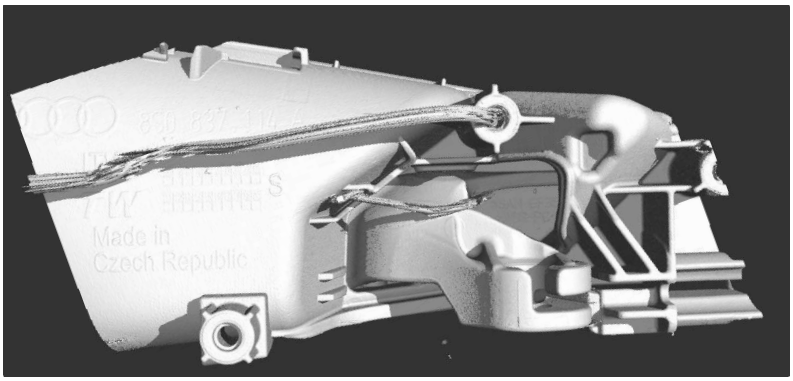

Figure 65: Rendered model of car handle inside heating chamber. The thermocouple cable is a bit blurred due to artefacts that occur near metal components.

From both datasets, at 20 °C and at 80 °C was calculated the surface. Both models were then superimposed and the surface comparison was carried out. VG studio tried to superimpose both surfaces to obtain best fit (best fit registration) but as we could see in figure 66 some surfaces were overlapped with no error and some were shifted very roughly. Manner of this shift was not probably caused by thermal changes but more likely by the noise in dataset. Since the software tried to overlap surfaces of both models with possible lowest error, but as the surface wasn't sharp without defects, fit errors may have occurred.

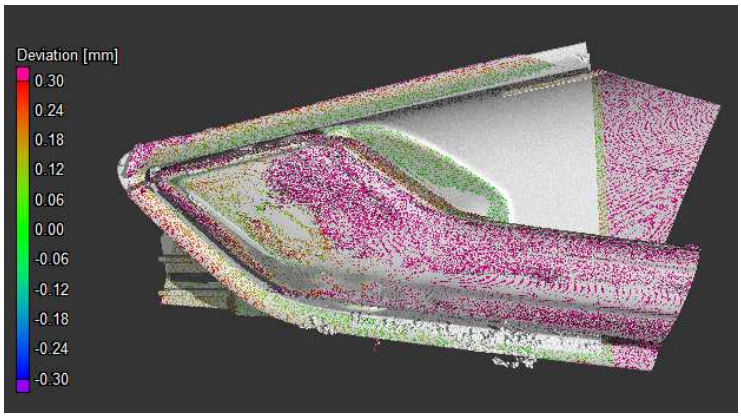

Figure 66: Overlapped surfaces of both datasets with errors. The green points present a perfect match of surfaces while the pinky ones are shifted more than pre-set scale (0.3 mm).

In the figure 67 we can see a comparison of the plastic housing in slice. The surface of the reference scan (at 20 °C) seems to be shrink to the scan at 80 °C. That would be an expected result, but the manner and the magnitude of shift is beyond possible dilatation of material for this temperature difference. The housing of the chamber is from polyamid (concretely PA6 GF30). When we consider only linear expansion of material described by following equation:

$$\frac{L_h - L_0}{L_0} = \alpha \Delta T \tag{37}$$

Where the L_0 represents the length at room temperature and L_h is length after heating. The rate of elongation due to temperature difference ΔT is described by expansion coefficient α. The coefficient for polyamid moves from 20 to $30 \times 10^{-6}\,\mathrm{K}^{-1}$ [39]. It represents a shift within 0.12 or 0.18 % for thermal difference of 60 °C, which means for an approx. 5 cm wide handle shift in about 0.06 or max 0.09 mm.

Naturally we haven't considered the shape of the handle that could possibly cause local expansion exceed these values. Nevertheless, the observed shift is probably a combination of wrong fit and thermal expansion.

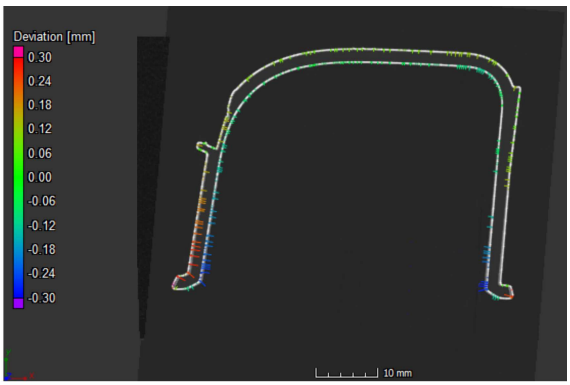

Figure 67: Comparison of plastic housing in slice. The reference model is shrunk to the heated one as expected. However, the amount of mismatch is mostly caused by wrong surface fitting instead of thermal dilatation.

10.3 −40 °C vs 80 °C

Unfortunately like the scan at room temperature also the scan at −40 °C was damaged by blurred edges due to the presence of sponge fragments. We tried to clean the surface and make it sharper for the comparison with scan at 80 °C. The result of comparison can be seen in figure 69.

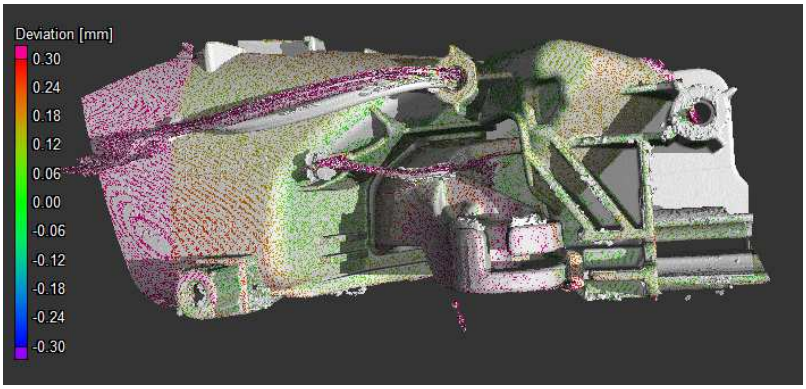

Figure 68: Comparison of models obtained at −40 °C vs scan at 80 °C. We can see that while some surfaces are overlapped without error (green places), some are shifted against each other out of the scale (pink places)

According to known thermal expansion coefficients, for temperature difference of 120 °C the expansion should be in range from 0.24 to 0.36 %. The handle could then elongate maximally 0.18 mm (considering 5 cm wide). Naturally the final expansion depends strongly also on the shape of the handle.

Investigation of the same part as in figure 69 but exposed to a higher temperature difference revealed similar scenario as before (figure 69). As the reference the scan at −40 °C was taken, we again observe that the cold handle seems to shrink in comparison to the hot one. On th other hand, on most places the expansion exceed the calculated values of shift.

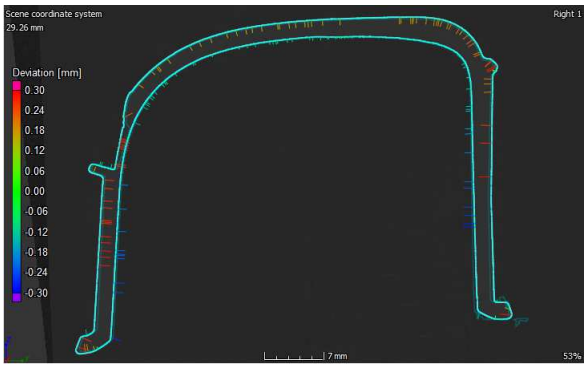

Figure 69: Comparison of the same part as in figure 69

10.4 Discussion of results

10.4.1 Freezing temperatures

We scanned the car door handle at different temperatures and observed the response of the material. Scan at freezing temperature (−40 °C) took place in polystyrene chamber. The handle in this chamber was surrounded by two sponges for insulation but also to keep stable position during scan. This solution helped to solve problems with thermal stability, but on the other side the similarity of attenuation coefficient of sponges and the handle caused problems with surface determination. In the case of the surface determination of scanned model the sponge caused fragments (figure 58) that had to be removed manually.

As we had relatively sharp surface of both scans at different temperatures we could move to the comparison. The comparison revealed the shift of material due to thermal changes. Similar shifts were already observed by Tomáš Koutecký [36].

10.4.2 Hot temperatures

Scan of the hot handle was carried out in a different chamber and in another position (the same parameters of scan). The obtained model was much better and with sharper edges. However, as the surface of the 80 °C scan was overlapped over the previous scan a relatively big errors occurred. Some places overlapped perfectly but some were mismatched over the range. Although at some places the amount of shift in range was calculated from linear expansion model, the distribution of the shifts suggest to fit errors rather than thermal expansion. Therefore the proper shape-change analysis cannot be calculated since we couldn't differ between fit error and thermal expansion. For a further comparison we should get a set of scans for every case and calculate an average surface that would serve as a standard for comparison with error calculations.

11 Conclusion

This diploma work handles the field of temperature controlled tomography. Th main goal of this work is to present available solutions that have already been used and describe problems and complications connected with every approach. Using obtained knowledge, design original solution for computed tomography at freezing temperatures on GE phoenix v|tome|x L240 computed tomography scanner.

The concept of computed tomography with its historical background is presented within the frame of this work. A part of this work is also about X-ray production and detection. Besides, the mechanism of image reconstruction using parallel X-ray beam is represented here. Since the work involves computation of heat transfer through designed chamber, the simplified heat transfer mechanism is here also explained.

However, the main part of the work is experimental. The entire process from testing the prototype of cooling chamber to a working solution is described here step by step. Although the work is focused on a solution enabling scanning at $-40\,°C$, the idea was moved further.The chamber not only for $-40\,°C$ but also for $80\,°C$ measurements. Since for heat chamber a completely different approach had to be chosen, the experiments that we carried out showed a satisfying thermal stability in range of $0.5\,°C$ and we came with working prototypes of cooling and heating chamber.

At the end, there are compared scanned data of a car handle that was kept at these extreme temperatures. And also the changes in material and in the shape of handle after exposure to the different temperatures are discussed.

References

[1] O. Glasser. *Wilhelm Conrad Röntgen and the Early History of the Roentgen Rays*. Norman Radiology Series. Norman Pub., 1993.

[2] Robert Cierniak. *X-Ray Computed Tomography in Biomedical Engineering*. Springer, 2011.

[3] A. M. Cormack. Representation of a function by its line integrals, with some radiological applications. *ournal of Applied Physics*, 1963.

[4] O.A. Laudal and R. Piene. *The Legacy of Niels Henrik Abel: The Abel Bicentennial, Oslo, 2002*. SpringerLink : Bücher. Springer Berlin Heidelberg, 2011.

[5] S. Helgason. *The Radon Transform*. Progress in Mathematics. Birkhäuser Boston, 1999.

[6] Marshall Cavendish Corporation. *Inventors and Inventions*. Number zv. 2 in Gale virtual reference library. Marshall Cavendish, 2008.

[7] Thorsten M. Buzug. *Computed Tomography : From Photon Statistics to Modern Cone-Beam CT*. Springer-Verlag Berlin Heidelberg, 2008.

[8] O.W. Richardson. *Thermionic Emission from Hot Bodies*. WATCHMAKER PUB, 2003.

[9] D.B. Williams and C.B. Carter. *Transmission Electron Microscopy: A Textbook for Materials Science*. Number zv. 2 in Cambridge library collection. Springer, 2009.

[10] F. R. Elder, A. M. Gurewitsch, R. V. Langmuir, and H. C. Pollock. Radiation from electrons in a synchrotron. *Phys. Rev.*, 71:829–830, Jun 1947.

[11] Richard A. Ketcham and Romy D. Hanna. Beam hardening correction for x-ray computed tomography of heterogeneous natural materials. *Computers and Geosciences*, 67:49 – 61, 2014.

[12] R. Behling. *Modern Diagnostic X-Ray Sources: Technology, Manufacturing, Reliability*. CRC Press, 2015.

[13] D.R. Dance. *Diagnostic Radiology Physics: A Handbook for Teachers and Students*. 2014.

[14] High {DQE} performance x-and gamma-ray fast imagers:: Emergent concepts. *Nuclear Instruments and Methods in Physics Research Section A: Accelerators, Spectrometers, Detectors and Associated Equipment*, 422(1–3):649 – 655, 1999.

[15] S.P. Hau-Riege. *High-Intensity X-rays - Interaction with Matter: Processes in Plasmas, Clusters, Molecules and Solids*. Wiley, 2012.

[16] G. Olafsson, E.T. Quinto, and American Mathematical Society. *The Radon Transform, Inverse Problems, and Tomography: American Mathematical Society Short Course, January 3-4, 2005, Atlanta, Georgia*. AMS Short Course Lecture Notes. American Mathematical Society, 2006.

[17] L. Debnath and D. Bhatta. *Integral Transforms and Their Applications, Second Edition*. CRC Press, 2006.

[18] J. Radon. Über die Bestimmung von Funktionen durch ihre Integralwerte längs gewisser Mannigfaltigkeiten. *Akad. Wiss.*, 69:262–277, 1917.

[19] J. Hsieh. *Computed Tomography: Principles, Design, Artifacts, and Recent Advances*. SPIE Press monograph. SPIE Press, 2003.

[20] T. Lestina and R.W. Serth. *Process Heat Transfer: Principles, Applications and Rules of Thumb*. Elsevier Science, 2010.

[21] T.L. Bergman, F.P. Incropera, D.P. DeWitt, and A.S. Lavine. *Fundamentals of Heat and Mass Transfer*. Wiley, 2011.

[22] Thomas De Schryver, Marijn Boone, Tim De Kock, Bert Masschaele, Manuel Dierick, and Luc Van Hoorebeke. A compact, low cost cooling stage for x-ray micro-ct setups. In *Industrial Computed Tomography, 5th Conference, Abstracts*, 2014.

[23] R.M. Lieb-Lappen, E.J. Golden, and R.W. Obbard. Metrics for interpreting the microstructure of sea ice using x-ray micro-computed tomography. *Cold Regions Science and Technology*, 138:24 – 35, 2017.

[24] D. Weiß, G. Schneider, B. Niemann, P. Guttmann, D. Rudolph, and G. Schmahl. Computed tomography of cryogenic biological specimens based on x-ray microscopic images. *Ultramicroscopy*, 84(3-4):185–197, 2000.

[25] M. A. Le Gros, G. Mcdermott, B. P. Cinquin, E. A. Smith, M. Do, W. L. Chao, P. P. Naulleau, and C. A. Larabell. Biological soft x-ray tomography on beamline 2.1 at the advanced light source. *Journal of Synchrotron Radiation*, 21(6):1370–1377, 2014.

[26] T. Beetz, M.R. Howells, C. Jacobsen, C.-C. Kao, J. Kirz, E. Lima, T.O. Mentes, H. Miao, C. Sanchez-Hanke, D. Sayre, and D. Shapiro. Apparatus for x-ray diffraction microscopy and tomography of cryo specimens. *Nuclear Instruments and Methods in Physics Research Section A: Accelerators, Spectrometers, Detectors and Associated Equipment*, 545(1–2):459 – 468, 2005.

[27] Günter Schmahl, Dietbert Rudolph, Peter Guttmann, Gerd Schneider, Jürgen Thieme, and Bastian Niemann. Phase contrast studies of biological specimens with the x-ray microscope at bessy (invited). *Review of Scientific Instruments*, 66(2):1282–1286, 1995.

[28] Gerry McDermott Mark A. Le Gros Christian G. Knoechel Maho Uchida Carolyn A. Larabell. Soft x-ray tomography and cryogenic light microscopy: The cool combination in cellular imaging. *Trends in Cell Biology*, 19(11):587–595, October 7 2009.

[29] Gerd Schneider. Cryo x-ray microscopy with high spatial resolution in amplitude and phase contrast. *Ultramicroscopy*, 75(2):85 – 104, 1998.

[30] Marian Kampschulte, Georg Erdmann, Jonas Sender, Gunhild Martels, Wolfgang Böcker, Thaqif ElKhassawna, Christian Heiß, Alexanders Claus Langheinrich, Elke Roeb, Martin Roderfeld, and Gabriele Anja Krombach. The development and validation of micro-ct of large deep frozen specimens. *Scanning*, 37(1):63–72, 2015.

[31] Enyu Guo, Guang Zeng, Daniil Kazantsev, Peter Rockett, Julian Bent, Mark Kirkland, Gerard Van Dalen, David S. Eastwood, David StJohn, and Peter D. Lee. Synchrotron x-ray tomographic quantification of microstructural evolution in ice cream - a multi-phase soft solid. *RSC Adv.*, 7:15561–15573, 2017.

[32] Julie L. Fife, Michel Rappaz, Mattia Pistone, Tine Celcer, Gordan Mikuljan, and Marco Stampanoni. Development of a laser-based heating system for *in situ* synchrotron-based X-ray tomographic microscopy. *Journal of Synchrotron Radiation*, 19(3):352–358, May 2012.

[33] M. Mukherjee, U. Ramamurty, F. Garcia-Moreno, and J. Banhart. The effect of cooling rate on the structure and properties of closed-cell aluminium foams. *Acta Materialia*, 58(15):5031 – 5042, 2010.

[34] J. Desrues, G. Viggiani, and P. Bésuelle. *Advances in X-ray Tomography for Geomaterials*. ISTE. Wiley, 2010.

[35] W. Liu and M. Pecht. *IC Component Sockets*. Wiley, 2004.

[36] T. Koutecký, T. Zikmund, D. Glittová, D. Paloušek, J. Živčák, and J. Kaiser. X-ray micro-ct measurement of large parts at very low temperature. *Review of Scientific Instruments*, 88(3):033707, 2017.

[37] M. Biron. *Thermoplastics and Thermoplastic Composites: Technical Information for Plastics Users*. Elsevier Science, 2007.

[38] Rosaria Conti, Aurelio Agliolo Gallitto, and Emilio Fiordilino. Measurement of the convective heat-transfer coefficient. *The Physics Teacher*, 52(2):109–111, 2014.

[39] VDI Gesellschaft. *VDI Heat Atlas*. VDI-Buch. Springer Berlin Heidelberg, 2010.